(4)

AFGL-TR-88-0204

Research in Geodesy and Geophysics Based Upon Radio Interferometric Observations of Extragalactic Radio Sources

T. A. Herring

Harvard College Observatory
60 Garden Street
Cambridge, MA 02138

1 October 1988

Final Report
3 April 1986-15 June 1988

AIR FORCE GEOPHYSICS LABORATORY
AIR FORCE SYSTEMS COMMAND
UNITED STATES AIR FORCE
HANSCOM AIR FORCE BASE, MASSACHUSETTS 01731-5000

Unclassified
SECURITY CLASSIFICATION OF THIS PAGE

AD-A200 858

REPORT DOCUMENTATION PAGE

1a. REPORT SECURITY CLASSIFICATION: Unclassified	1b. RESTRICTIVE MARKINGS
2a. SECURITY CLASSIFICATION AUTHORITY	3. DISTRIBUTION/AVAILABILITY OF REPORT: Approved for public release; distribution unlimited
2b. DECLASSIFICATION/DOWNGRADING SCHEDULE	
4. PERFORMING ORGANIZATION REPORT NUMBER(S)	5. MONITORING ORGANIZATION REPORT NUMBER(S): AFGL-TR-88-0204
6a. NAME OF PERFORMING ORGANIZATION: Harvard College Observatory; 6b. OFFICE SYMBOL (If applicable)	7a. NAME OF MONITORING ORGANIZATION: Air Force Geophysics Laboratory (LWG)
6c. ADDRESS (City, State and ZIP Code): 60 Garden Street, Cambridge, MA 02138	7b. ADDRESS (City, State and ZIP Code): Hanscom Air Force Base, Massachusetts 01731-5000
8a. NAME OF FUNDING/SPONSORING ORGANIZATION: Air Force Geophysics Laboratory; 8b. OFFICE SYMBOL (If applicable): LWG	9. PROCUREMENT INSTRUMENT IDENTIFICATION NUMBER: F19628-86-K-0025
8c. ADDRESS (City, State and ZIP Code): Hanscom Air Force Base, MA 01731-5000	10. SOURCE OF FUNDING NOS.

PROGRAM ELEMENT NO.	PROJECT NO.	TASK NO.	WORK UNIT NO.
61102F	2309	GI	BM

11. TITLE (Include Security Classification): Research in Geodesy and Geophysics Based Upon Radio Interferometric Observations of Extragalactic Radio Sources

12. PERSONAL AUTHOR(S): T.A. Herring

13a. TYPE OF REPORT	13b. TIME COVERED	14. DATE OF REPORT (Yr., Mo., Day)	15. PAGE COUNT
Final	FROM 4/3/86 TO 6/15/88	88/10/01	82

16. SUPPLEMENTARY NOTATION

17. COSATI CODES			18. SUBJECT TERMS (Continue on reverse if necessary and identify by block number)
FIELD	GROUP	SUB. GR.	Plate tectonics; Kalman Filtering.

19. ABSTRACT (Continue on reverse if necessary and identify by block number)

See reverse side for abstract.

20. DISTRIBUTION/AVAILABILITY OF ABSTRACT: UNCLASSIFIED/UNLIMITED ☐ SAME AS RPT. ☐ DTIC USERS ☐	21. ABSTRACT SECURITY CLASSIFICATION: Unclassified
22a. NAME OF RESPONSIBLE INDIVIDUAL: Vishnu Nevrekar, Capt. USAF	22b. TELEPHONE NUMBER (Include Area Code); 22c. OFFICE SYMBOL: AFGL/LWG

DD FORM 1473, 83 APR EDITION OF 1 JAN 73 IS OBSOLETE.

Unclassified
SECURITY CLASSIFICATION OF THIS PAGE

Abstract

We have used data from the Mark III very-long-baseline interferometry (VLBI) system to study the relative motions of radiotelescopes on the Pacific, North American, and Eurasian plates, and in the deformation zone between the North American and Pacific plates in the California region. These results are in accord with recent geologic plate motion models, and a distributed deformation zone between the North American and Pacific plates. We have carried out a number of studies on the accuracy of the results being obtained with VLBI. The most notable of these studies are of the repeatability of the estimates of three-dimensional coordinates of the sites for long baselines ($\approx$4,000 km), and the effects of calibrations of the "wet" tropospheric delays using water-vapor radiometers. We have also been studying the usefulness of observations made at very low elevation angles ($\approx 4^{\circ}$) for improving the accuracy of VLBI baseline determinations. We have also studied the forced nutations of the Earth which yielded results consistent with the flattening of the core-mantle boundary being about 5% greater than that predicted by the assumption of hydrostatic equilibrium within the Earth. The effects of ocean tides and the anelasticity of the mantle on the forced nutations are not clearly evident in our results, and are still being investigated.

CONTENTS

Significant Accomplishments

Under this contract we have been examining many facets of the geodetic and geophysical applications of very-long-baseline interferometry (VLBI). In the following sections we present a summary of the results which have been obtained. In the appendices to this report we present a detailed discussion of the procedures we are using in our Kalman filter VLBI data analysis software, and we include pre- and reprints of the papers we have published under this contract (Davis *et al.*, 1988; Elgered *et al.*, 1988; Herring *et al.*, 1988; Herring ,1988)

Global site velocity estimates

For our analysis of the VLBI data set, we combined 532 experiments carried out between July 1980 and June 1987. This data set contained 202,051 group delay measurements. From 21,245 estimates of site positions, 189 global parameters were estimated. We restricted the sites used in this analysis to those which had been used five or more times during the last seven years. The global parameters consisted of 31 site position estimates and 30 site velocity estimates. (One site was used for only a one week period, and, hence, no velocity was estimated for this site). We estimated all site positions and velocities (except as noted above) with weak *a priori* constraints applied to these quantities (± 1 meter for positions, and ± 1 meter/year for velocities). In addition, we allowed the position of the earth's rotation axis and the value of UT1-AT to change randomly between experiments. When all of the experiments are combined in this fashion, the final estimates of the site position and velocities have large absolute uncertainties because the coordinate system in which they are given is not well defined. Since all sites were allowed to move, and the changes in the earth orientation parameters were weakly constrained, the coordinate system in which the final results are given can translate and rotate relative to its position and orientation at the epoch of the first experiment in the solution. To remove this rank deficiency in the final results we need to adopt the values for three scalars to represent a general translation, and three scalars to represent a general rotation of the coordinate system, relative to its initial position and orientation. There are no unique values for these six parameters, although there are a number of methods we could adopt for obtaining values of these parameters. For example, the motion of one site could be adopted as a reference in order to determine the translation of the coordinate system, and the earth orientation values from an earth orientation service (such as BIH or IRIS) could be

adopted to define the final orientation of the coordinate system. However, these types of techniques do not provide a very satisfactory solution to the problem. If the motion of the reference is different from the adopted motion, then the difference will be applied to all other sites in the network, thus leading to apparent motions at these sites. The adoption of earth orientation values from BIH or IRIS also presents problems because neither of these services currently includes site motions in its determinations of the earth orientation parameters.

The procedure we have adopted for determining the three translation and three rotation parameters is to estimate their values by minimizing the root-mean-square (RMS) difference between the estimated (locally) horizontal velocities and the predicted velocities from a global plate motion model for a selected set of sites. To resolve the rank deficiency for this initial solution, we used the Minster and Jordan RM2 plate motion model, and the velocities of 11 of the 30 sites whose velocities were estimated. These eleven sites were selected because of their geographical coverage of the VLBI network, and the frequency of their use during the seven years spanned by the VLBI data set. The estimated velocties and their one sigma standard deviations, and the RM2 velocities for all 30 sites, are given in Table 1. These results are also presented in graphical form in Figures 1-3. The figures clearly show a pattern of motion which is very consistent with the RM2 plate motion model except in the transition region between the North American and Pacific plates along the San Andreas fault. Even here, the motions seem to show a smooth change between North American velocities and Pacific velocities.

There were some unexpected results which came out of this solution. The relative (horizontal) motions of the VLBI sites in Eastern North America, including Ft. Davis, TX, are all very small, and consistent with zero within their 90% confidence intervals. This result was surprising because the length of the baseline between the Westford, MA, and the Ft. Davis, TX, sites has been decreasing on average by $\approx$7 mm/yr for the last seven years, although there have been a number of excursions from this average rate. For the last year, the length has shown no appreciable change, and during this interval the length is very similar to its value in 1980. In our global solution, this decreasing baseline length is due mainly to vertical motions at the Ft. Davis site. (For the Westford-Ft. Davis baseline, $\approx$25% of the height change projects into the baseline length.) We are still investigating whether this height change is due to the motion of the site, or due to an inadequacy in our models of the tropospheric delay. All of the

TABLE 1. Estimated velocities of VLBI sites obtained from the analysis discussed in the text.

Site	ϕ (deg)	λ (deg)	Estimates North Vel. (mm/yr)	Estimates East Vel. (mm/yr)	RM2 Predicted North Vel. (mm/yr)	RM2 Predicted East Vel. (mm/yr)	Plate‡
Haystack†,MA	42.6	288.5	-5.±2.	-22.±3.	-4.	-24.	NA
Westford†,MA	42.6	288.5	-5.±2.	-23.±3.	-4.	-24.	NA
Maryland Pt.,MD	38.4	282.8	-8.±9.	-19.±8.	-5.	-24.	NA
NRAO,WV	38.4	280.2	-13.±6.	-28.±5.	-6	-24.	NA
Richmond,FL	25.6	279.6	-10.±3.	-25.±3.	-6.	-25.	NA
Ft. Davis,TX	30.6	256.1	-8.±2.	-23.±2.	-9.	-23.	NA
Platville,CO	40.2	255.3	-19.±6.	-19.±5.	-9.	-22.	NA
Flagstaff,AZ	35.2	248.4	-6.±10.	-39.±9.	-10.	-21.	NA
Yuma,AZ	32.9	245.8	-10.±3.	-29.±3.	-10.	-21.	NA
Ely,NV	39.3	245.6	-16.±5.	-27.±4.	-10.	-20.	NA
Blackbutte,CA	33.7	244.3	19.±6.	-42.±5.	-10.	-21.	NA
Monument Peak,CA	32.9	243.6	19.±3.	-50.±2.	-10.	-21.	NA
Pinyon Flats,CA	33.6	243.5	17.±4.	-46.±3.	-10.	-21.	NA
Mojave†,CA	35.3	243.1	-3.±2.	-27.±2.	-10.	-21.	NA
Pearblossom,CA	34.5	242.1	8.±7.	-38.±5.	-10.	-21.	NA
Pasadena,CA	34.2	241.8	1.±3.	-46.±2.	-10.	-21.	NA
Owens Valley†,CA	37.2	241.7	-4.±2.	-28.±2.	-10.	-21.	NA
Mammouth Lakes,CA	37.6	241.1	-3.±5.	-30.±3.	-10.	-21.	NA
Vandenberg†,CA	34.6	239.3	26.±2.	-56.±2.	35.	-55.	PA
Quincy,CA	40.0	239.1	-4.±3.	-28.±3.	-10.	-20.	NA
Hatcreek†,CA	40.8	238.5	-3.±2.	-26.±2.	-10.	-20.	NA
Ft. Ord,CA	36.7	238.2	28.±6.	-49.±5.	-10.	-21.	NA
Presidio,CA	37.8	237.5	15.±8.	-42.±6.	-10.	-21.	NA
Gilmore Ck.†,AK	65.0	212.5	-15.±3.	-8.±3.	-10.	-8.	NA
Kauai†,HI	22.1	200.3	44.±5.	-79.±4.	53.	-85.	PA
Kwajalean†	9.4	167.5	53.±9.	-90.±8.	49.	-97.	PA
Kashima†, Japan	36.0	140.1	9.±8.	-21.±8.	-2.	-13.	NA
Wettzell†, FRG	49.1	12.9	2.±3.	5.±4.	0.	0.	EU
Onsala†, Sweden	57.4	11.9	0.±3.	-1.±4.	0.	0.	EU

‡ The abbreviations of the tectonic plate names are NA–North America, PA–Pacific, and EU–Eurasia. The velocities are arbitrarily referred to the Eurasian plate.

† These sites were used in the determination of the translation and the orientation of the coordinate system (see text for discussion).

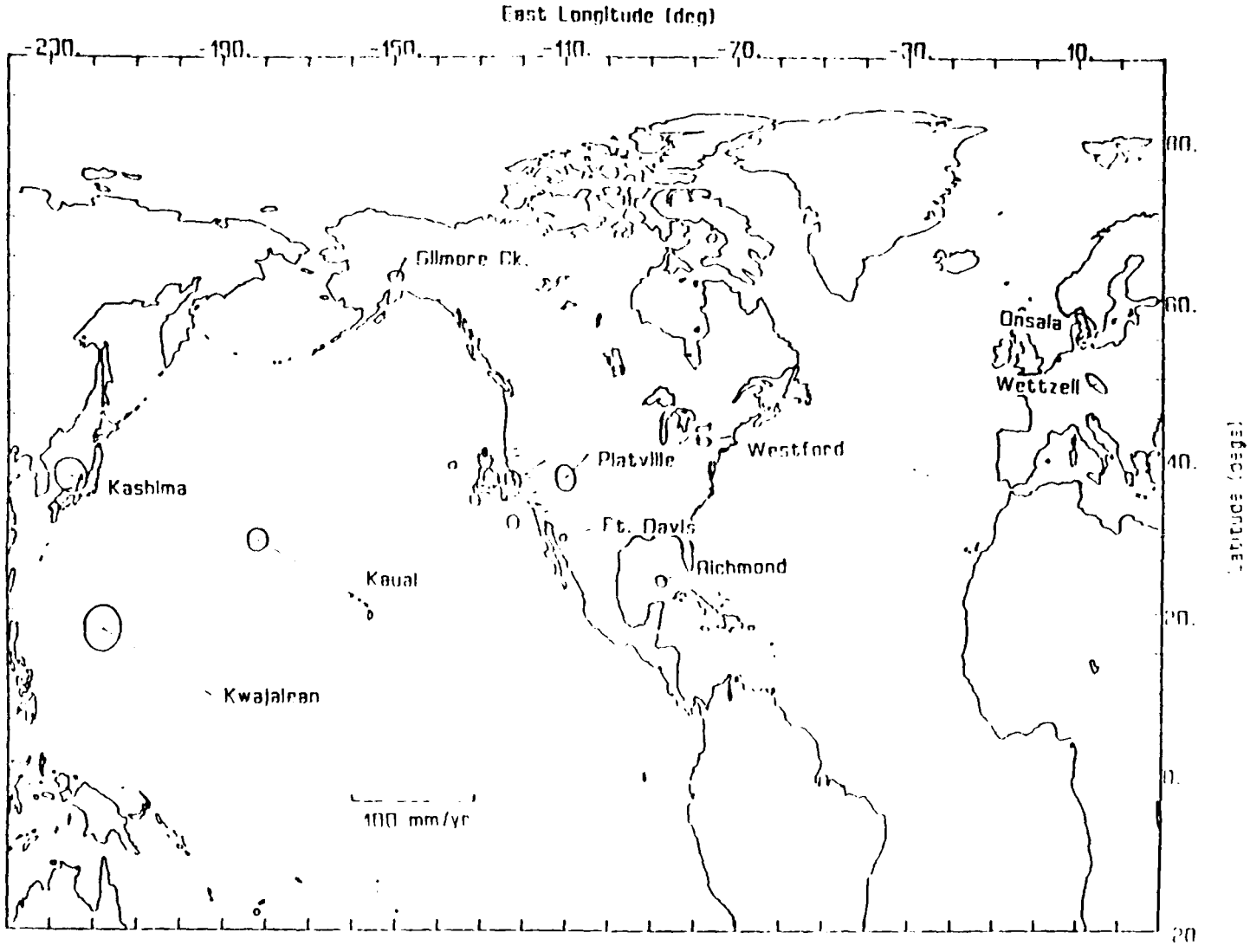

Figure 1. Vector motions of the VLBI sites given in Table 1. The error ellipses give 90% confidence limits.

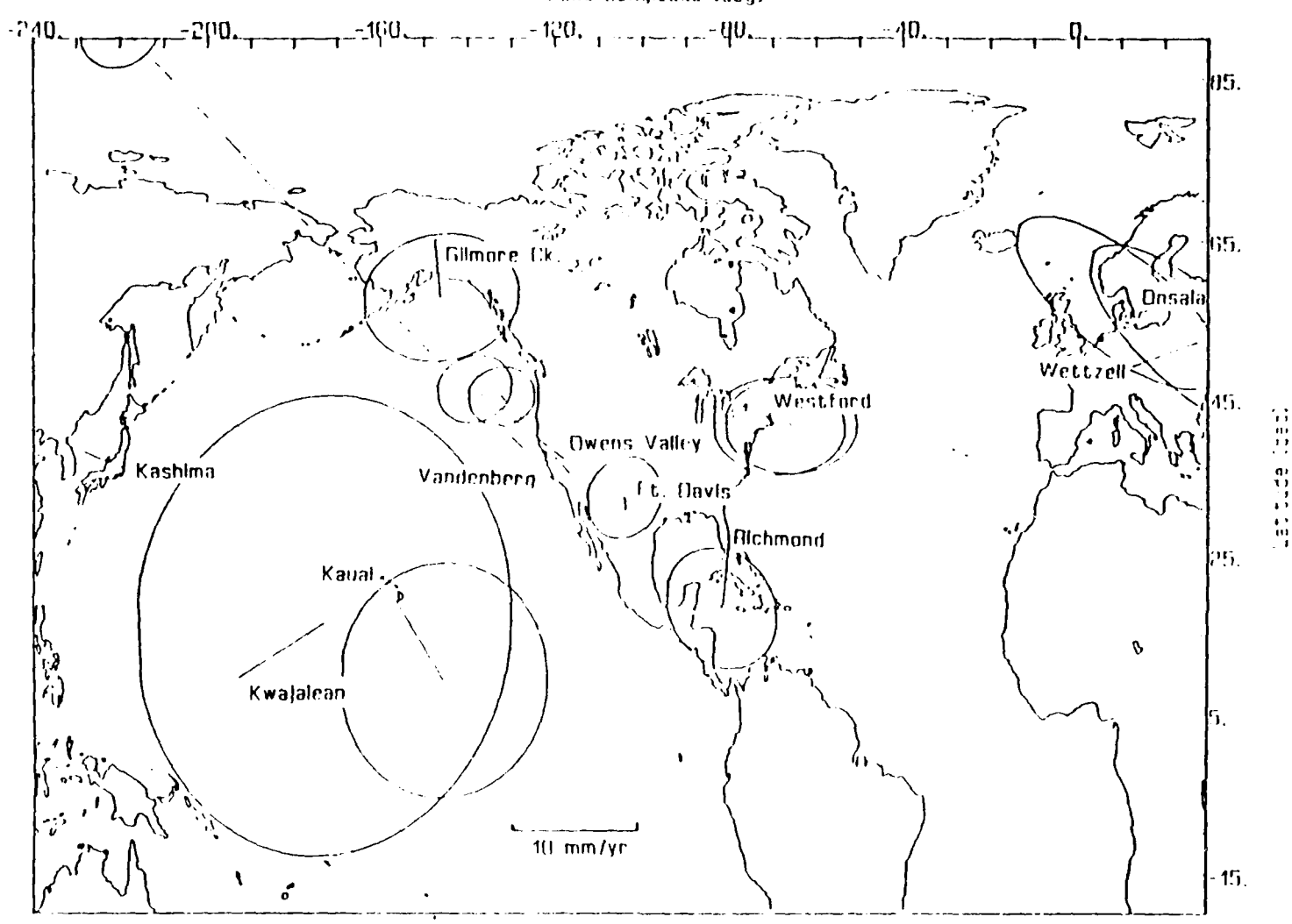

Figure 2. Vector motions of the VLBI sites given in Table 1 with the RM2 plate motion model removed. (Only selected sites are shown in the region of California, see Figure 3.). The error ellipses give 90% confidence limits. Note the change in scale for this figure.

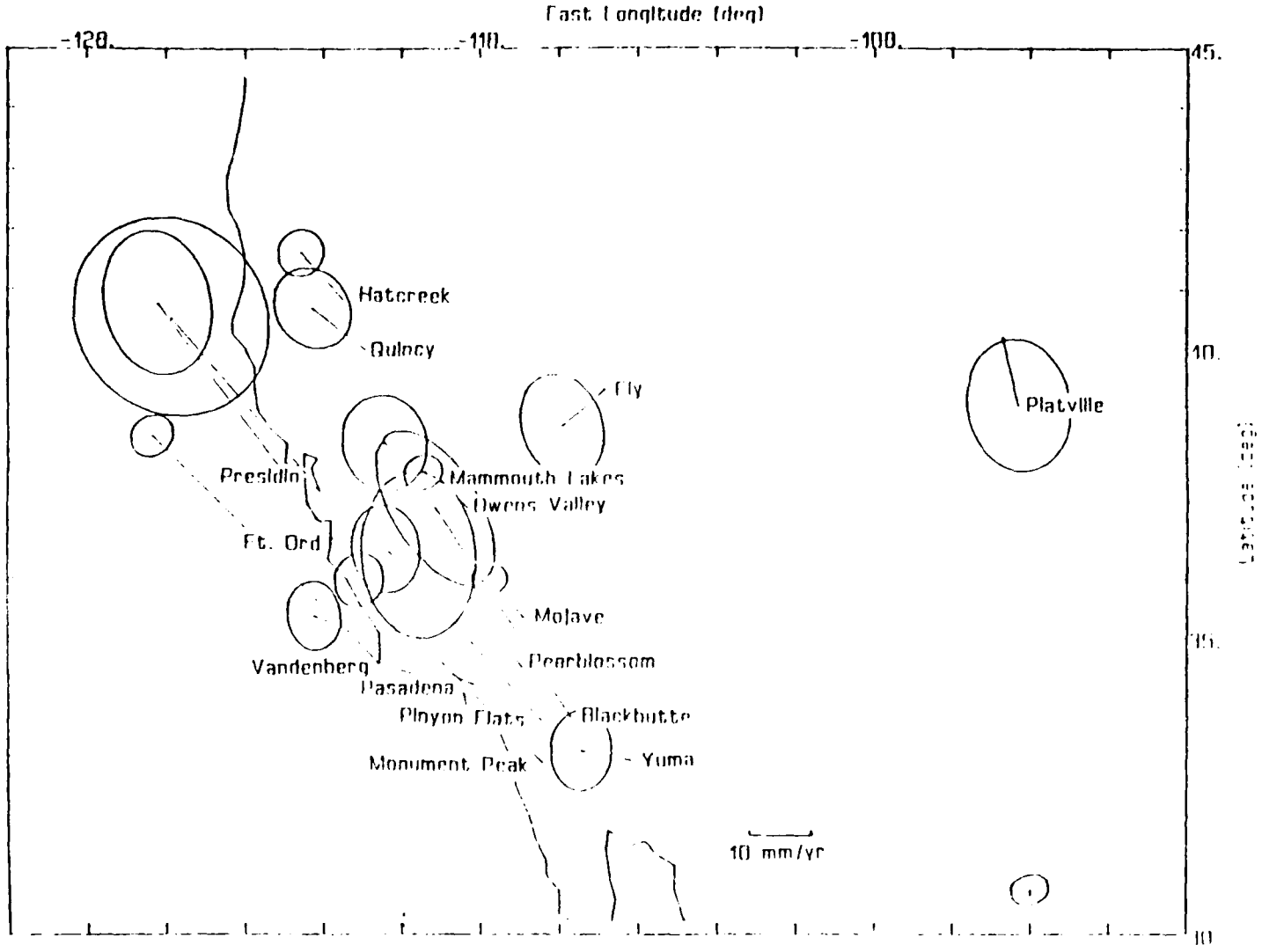

Figure 3. Vector motions of the VLBI sites in the region of California with the RM2 North American plate velocities removed. The error ellipses give 90% confidence limits.

other frequently observed VLBI sites have vertical velocities of less than 10 mm/yr with standard deviations of typically a few mm/yr. Our analysis also shows that the VLBI sites at Mojave, Owens Valley, Hatcreek, Mammouth Lakes, and Quincy are all moving relative to North America with velocities which are consistent with the extension of the Basin and Range Province of California.

Three-dimensional coordinates

In the past we have not used three-dimensional coordinates for tectonic-motion studies because the coordinate system in which these values are determined is fixed with respect to the rotation axis of the Earth. This axis moves relative to the crust of the Earth. The motion of the rotation axis can be as large as 12 meters during a 12 month interval, and hence must be accurately accounted for in any study of changes in the three-dimensional coordinates of VLBI sites. Conventional geodetic techniques are not accurate enough for us to be able to use their measurements of the position of the Earth's rotation axis for tectonic-motion studies. However, now that modern geodetic techniques, such as very-long-baseline interferometry (VLBI), satellite laser ranging (SLR) and lunar laser ranging (LLR), are being used to monitor the motions of the Earth's rotation axis, we can now consider using three-dimensional coordinates for tectonic-motion studies.

To test the accuracy of the Earth rotation measurements obtained from modern techniques we have been studying the repeatability of the estimates of the coordinates of the VLBI site in the Mojave desert obtained from the VLBI experiments being used to test the usefulness of observations taken at low-elevations angles. These experiments are often referred to as the "LOWEL" experiments. We have concentrated on comparing the results from two different sets of Earth rotation measurements. One series of measurements, which we will refer to as the "CfA" series, was obtained from our analysis of all VLBI data except for those in the LOWEL experiments. The CfA series is a North America fixed system (*i e.*, in this system, sites not moving relative to the North American plate, should have constant coordinates). The other series, which we will refer to as the "JPL PRIME" series, was obtained at the Jet Propulsion Laboratory by combining Earth rotation data from Satellite Laser Ranging, Lunar Laser Ranging and Deep-Space Network VLBI data. The JPL PRIME series should have no rotation relative to the AM0-1 global plate model. Within this system, sites on the North American plate should move with a velocity of about 2 cm/yr. These two

series of Earth rotation values contain no common data. In Figures 4 and 5 we show the estimated positions of the Mojave site in the coordinate systems defined by these earth rotation series. The coordinates are shown in a (Mojave) local north, east and up (height) frame. The repeatability of the estimates of the Mojave coordinates is better with the CfA earth rotation values than with the JPL Prime series. The velocity of the Mojave site obtained when the CfA earth rotation series is used is consistent, within the uncertainties of these estimates, with the estimates of the Mojave velocity obtained from the global solutions discussed in previous reports. (These global solutions do not include the LOWEL experiments. The velocity estimates from these global solutions range between 0.9–0.7 N and -0.7 and -0.4 E cm/yr, depending on which sites are used to obtain the reference frame; see previous reports.)

We may use these results to assess the precision of the CfA and JPL PRIME earth rotation series. Most of the LOWEL experiments have been single baseline experiments using the Haystack Observatory or the Westford Observatory as the second site in the baseline. Since Haystack and Westford are only 1.24 kms apart, the sensitivity of the Mojave coordinates to changes in the Earth rotation parameters will be almost identical for these two baselines. When coordinates of either Haystack or Westford are fixed at their *apriori* values (to define the translation origin of the coordinate system), the sensitivity of the Mojave North, East and height estimates (δN, δE and δU) to changes in the Earth rotation parameters, δx, δy, and $\delta UT1$, is given by:

$$\begin{pmatrix} \delta N \\ \delta E \\ \delta U \end{pmatrix} = \begin{pmatrix} -14 & -1 & 9 \\ 3 & 1 & -9 \\ -12 & 3 & -13 \end{pmatrix} \begin{pmatrix} \delta x \\ \delta y \\ \delta UT1 \end{pmatrix} \tag{1}$$

where the coefficients for the matrix are computed for coordinate changes in mm and the orientation changes in mas. In addition, any errors in modeling the atmospheric delays at the Haystack/Westford site, which would normally affect the estimate of the height at these sites, will project into the coordinates of the Mojave site. For a height error of $\delta U_{H/W}$ at these sites, the effect on the estimates of the Mojave coordinates is be given by:

$$\begin{pmatrix} \delta N \\ \delta E \\ \delta U \end{pmatrix} = \begin{pmatrix} 0.25 \\ 0.53 \\ 0.90 \end{pmatrix} \delta U_{H/W}. \tag{2}$$

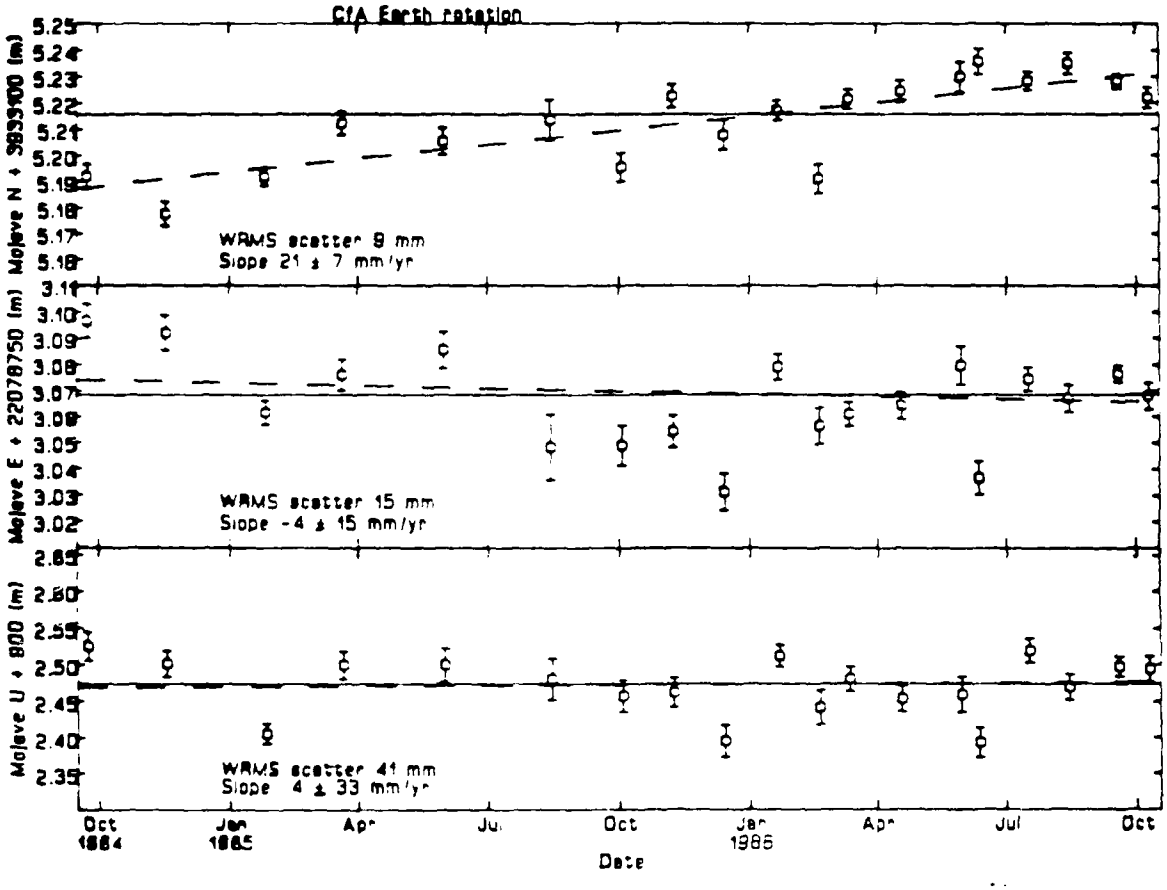

Figure 4. Estimated positions of the Mojave antenna from the LOWEL experiments with the orientation of the coordinate system defined by the CfA Earth rotation series (see text). The coordinate system is a (Mojave) North, East and Up frame, where N is the ellipsoidal arc distance from the equator, E is the distance from the Greenwich meridian along the small circle at the geodetic latitude of the site, and U is the height of the site above the ellipsoid. The error bars do not account for the uncertainty in the realization of the North American fixed coordinate system.

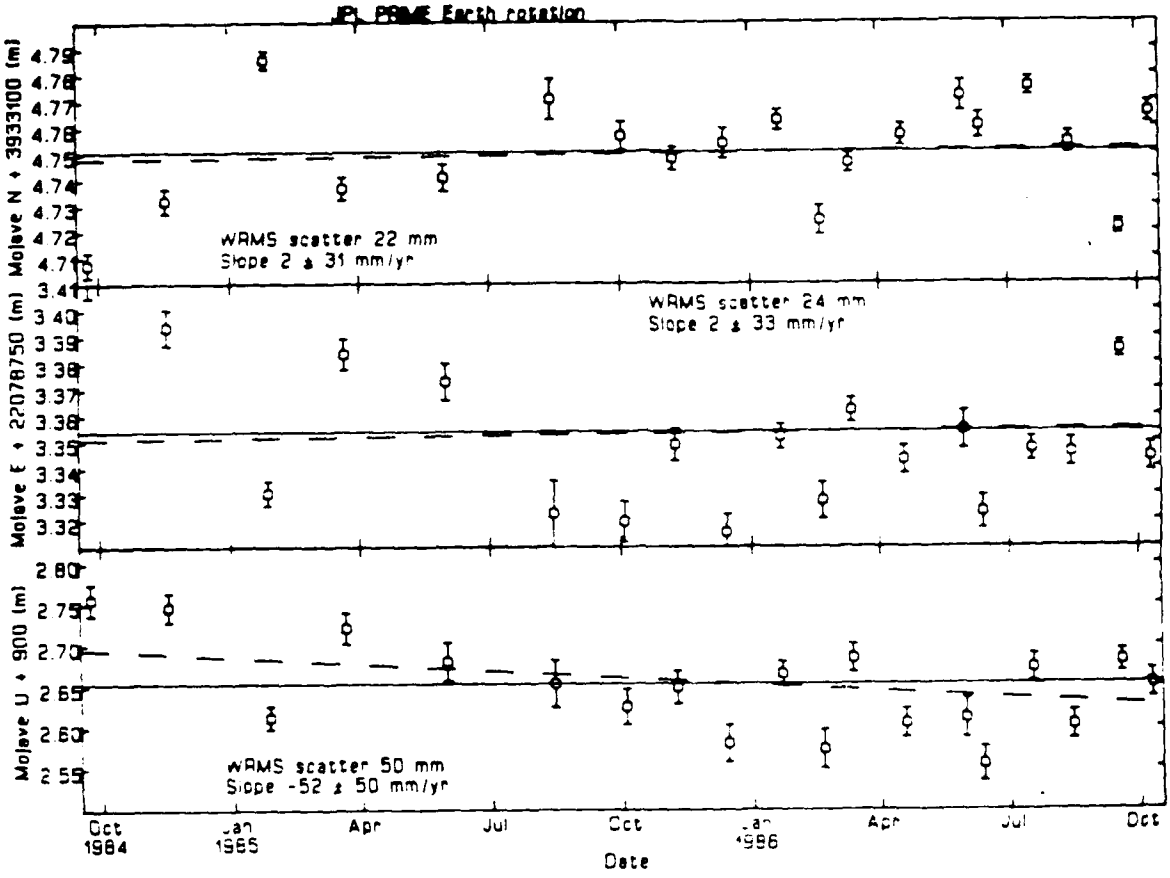

Figure 5. Estimated positions of the Mojave antenna from the LOWEL experiments with the orientation of the coordinate system defined by the JPL PRIME Earth rotation series (see text). See Figure 1 caption for definition of N, E and U.

If we assume that errors in the estimates of the North and East components of the Mojave site position are dominated by errors in the Earth rotation data and by errors in the height of Haystack/Westford, then we may use Equations 1 and 2 to estimate uncertainties of the Earth orientation values and $\delta U_{H/W}$. Such an analysis of the CfA results yields, assuming that the variances of the errors in each of the components of the Earth rotation parameters are equal, uncertainties of 0.4 mas for the Earth rotation parameters and 28 mm for $\delta U_{H/W}$. A similar analysis for the results obtained using the JPL PRIME series, yields 1.2 mas for the Earth rotation parameters and 40 mm for $\delta U_{H/W}$. This uncertainty of the JPL PRIME series is consistent with the quoted uncertainties for this series, and is confirmed by the direct comparison of the CfA and JPL PRIME series shown in Figure 6.

We plan to study further the usefulness of three-dimensional coordinates for studying tectonic motions. We will probably next process the Onsala–Wettzell ($\approx$1000 km) baseline using the CfA and the JPL PRIME earth rotation series, and assesses the precision with which differential position of these two sites can be determined.

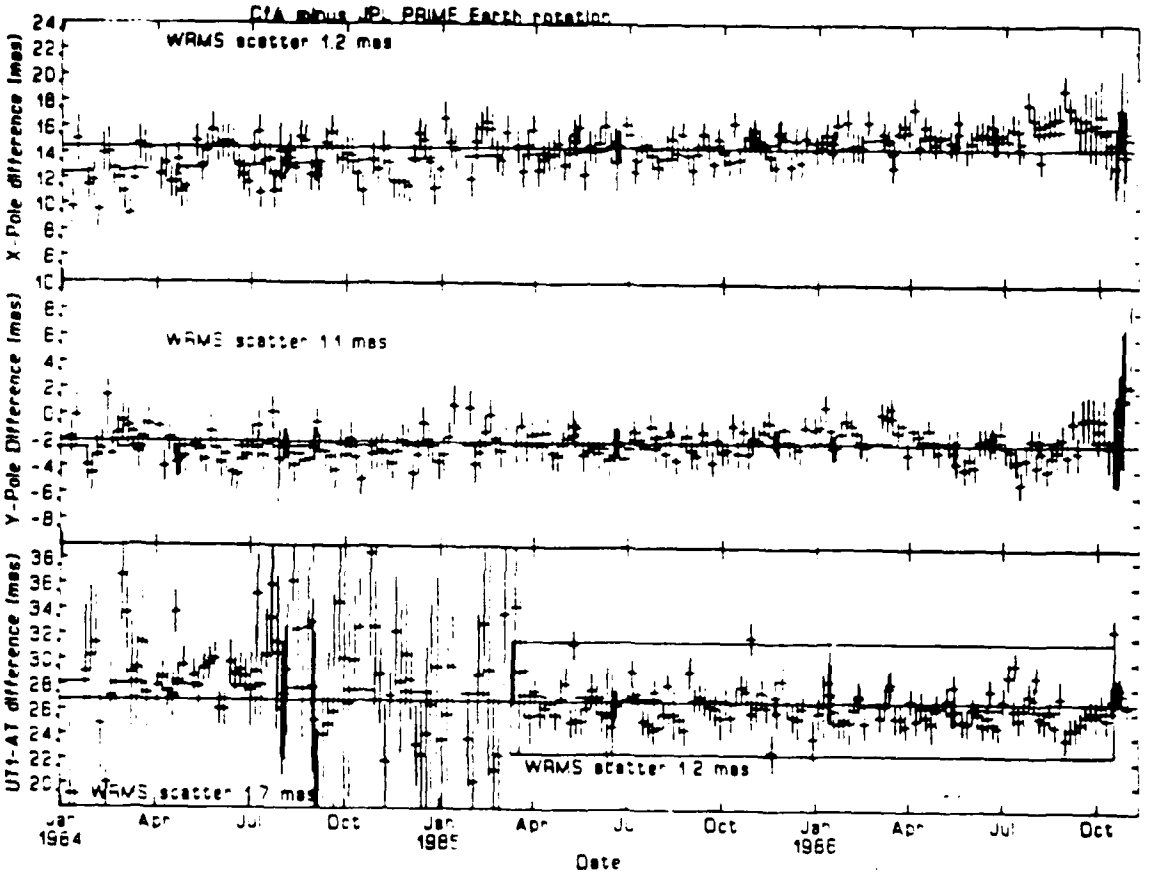

Figure 6. Differences between the CfA and JPL PRIME earth rotation series. The error bars are the root–sum–square of the standard deviations for each of the series. These error bars are dominated by the uncertainty in the JPL PRIME series.

Appendix A. Kalman filter estimator

We discuss here the basic set of matrix operations needed to implement a Kalman filter estimator. These equations appear in most text book which discuss Kalman filtering. The particular form we use is based on the works of Liebelt (1967) and Gelb (1974). We commence with the linearized form of the equations which relate VLBI observables to the parameters to be estimated:

$$y_t = \mathbf{A}_t x_t + v_t \qquad (A.1)$$

where all quantities refer to time t, and y_t is the vector of differences between the observations and their theoretical values calculated from *a priori* values of the parameters; x_t is the vector of adjustments to the *a priori* values of the parameters; $\mathbf{A}_t$ is the matrix of partial derivatives which relate the change in parameter values to changes in the values of the observables; and v_t is a vector of residuals which represent the noise in the observations. The dynamics of the parameters are represented by the state transition equation:

$$x_{t+1} = \mathbf{S}_t x_t + w_t \qquad (A.2)$$

where x_{t+1} is the vector of values of the parameters at time $t+1$; $\mathbf{S}_t$ is the state transition matrix at time t, *i.e.*, the matrix which gives the expected changes in the parameters between times $t+1$ and t; and w_t is the vector of random perturbations to the state. The elements of w_t corresponding to non-stochastic parameters are zero, *i.e.*, there are no perturbations of the state with time. These parameters typically, but not necessarily, include the positions of the radio telescopes and the radio sources, and the orientation of the terrestrial coordinate system in space. The stochastic parameters typically include the components of the random walks and integrated random walks being used to represent the fluctuations of the clocks and the atmospheric delays.

Equations (A.1) and (A.2) represent a general set of equations for linear dynamic system. In order to form the Kalman filter estimator we make the following assumptions:

$$\langle v_t \rangle = 0, \qquad \text{for all } t \qquad (A.3)$$

$$\langle v_t v_{t+j} \rangle = 0, \qquad \text{for all } j \neq 0 \qquad (A.4)$$

$$\langle v_t w_{t+j} \rangle = 0, \qquad \text{for all } t \text{ and } j \qquad (A.5)$$

$$\langle v_t x_{t+j} \rangle = 0, \qquad \text{for all } t \text{ and } j \qquad (A.6)$$

$$\langle w_t \rangle = 0, \qquad \text{for all } t \qquad (A.7)$$

$$\langle w_t w_{t+j} \rangle = 0, \qquad \text{for all } j \neq 0 \qquad (A.8)$$

$$\langle x_t w_{t+j} \rangle = 0, \qquad \text{for all } j > 0 \qquad (A.9)$$

We also define

$$\langle v_t v_t \rangle \equiv \mathbf{V_t} \tag{A.10}$$

$$\langle w_t w_t \rangle \equiv \mathbf{W_t} \tag{A.11}$$

The assumptions (A.5) and (A.6) ensures that the measurement process and the random motion of the system are uncorrelated. The assumptions (A.8) and (A.9) ensure that the current state of the system do not affect the random perturbations in the system at later times. For the classes of stochastic processes discussed in Appendix B this assumption is satisfied.

The Kalman filter estimation is carried out sequentially. The sequence for adding the observations at time $t+1$ to the estimation, given the state, $\hat{x}_t^t$, and its covariance matrix, $\mathbf{C_t^t}$, at time t is,

Prediction:

$$\hat{x}_{t+1}^t = \mathbf{S_t}\hat{x}_t^t \tag{A.12}$$

$$\mathbf{C_{t+1}^t} = \mathbf{S_t C_t^t S_t^T} + \mathbf{W_t} \tag{A.13}$$

Update:

$$\hat{x}_{t+1}^{t+1} = \hat{x}_{t+1}^t + \mathbf{K}(y_{t+1} - \mathbf{A_{t+1}}\hat{x}_{t+1}^t) \tag{A.14}$$

$$\mathbf{C_{t+1}^{t+1}} = \mathbf{C_{t+1}^t} - \mathbf{K A_{t+1} C_{t+1}^t} \tag{A.15}$$

where $\mathbf{K}$, the Kalman gain, is given by

$$\mathbf{K} = \mathbf{C_{t+1}^t A_{t+1}^T}(\mathbf{V_{t+1}} + \mathbf{A_{t+1} C_{t+1}^t A_{t+1}^T})^{-1} \tag{A.16}$$

Equations (A.12)–(A.16) form a complete sequence for adding observations into the filter. When the computations at time $t+1$ are completed, the sequence is repeated with quantities at time $t+2$ substituted for those at time $t+1$, and those at times $t+1$ for those at time t. The sequence is repeated until all observations have been included. To start the filter, *a priori* values for the parameters and their covariance matrix are used for quantities with sub– and superscript t. We refer to this sequence as the *forward* Kalman filter.

After all observations have been added to the forward Kalman filter, the final estimates of the non-stochastic parameters are determined. To determine the estimates of the stochastic parameters, a *backward* or *smoothing* Kalman filter solution must be performed. This is necessary because the estimates of stochastic parameter for all but the last epoch of observations do not contain the information about the parameters estimates supplied by later observations. Algorithms for the backward Kalman filter do not often appear in the literature. (This is because Kalman filters are most often used in real time applications, and only the values of the parameters at the current time of interest. Liebelt (1967, Chapter 6) gives an algorithm for the backward Kalman filter which requires relatively large amount of computer memory to implement. We have instead implemented the algorithm of Gelb (1974, Chapter 5).

The Gelb algorithm for smoothing takes the mean of the estimates of the parameters from the forward filter and from a forward filter with time running in reverse order. This mean is taken at an appropriate position in the filter equations such that when the mean is computed, all available information about the parameters is included. The mean is taken using the full covariance matrices for the forward and backward estimates of the parameters. The choice of exactly which positions in the filter equations are used to obtain the parameter estimates for taking the mean is arbitary provided that the condition that all information is used is satisfied. We have chosen the positions corresponding to Equations (A.14) and (A.15) for the forward running filter, and Equations (A.12) and (A.13) for the backward running filter. If a back solution is to be run (which is not always the case), then during the forward solution the parameter estimates and their covariance matrix at time $t+1$ are saved in a disk file. During the backward running filter, the smoothed estimates of the parameters are obtained after the prediction step from time $t+2$ to time $t+1$. (Note: that since the time is running backwards in this filter the observations from time $t+2$ are processed before those from time $t+1$.) The equations we use for taking the mean can be derived from the Kalman filter equations given above. They are

$$\mathbf{B} = \mathbf{C}_+(\mathbf{C}_- + \mathbf{C}_+)^{-1} \qquad (A.17)$$

$$\hat{x}_s = \hat{x}_+ + \mathbf{B}(\hat{x}_- - \hat{x}_+) \qquad (A.18)$$

$$\mathbf{C}_s = \mathbf{C}_+ - \mathbf{B}\mathbf{C}_+ \qquad (A.19)$$

where $\mathbf{B}$ is the Kalman filter gain for taking the mean; $\hat{x}_+$ and $\mathbf{C}_+$ are $\hat{x}_t^t$ and $\mathbf{C}_t^t$ from the forward running filter; $\hat{x}_-$ and $\mathbf{C}_-$ are $\hat{x}_t^{t+1}$ and $\mathbf{C}_t^{t+1}$ from the backward running filter; $\hat{x}_s$ and $\mathbf{C}_s$ are the smoothed estimates of the parameters and their covariance matrix at time t.

To implement the smoothing filter rigorously the Kalman filter equations should should be written in a more symmetrical form than that given by Equations (A.12)–(A.16), *i.e.,* an *a posterori* contraint should be placed on the parameter estimates after all of the observations have been included. The *a posterori* constraint would then be used as the *a priori* constraint when the backward running filter is started. We have not implemented the smoothing equations in this manner. Instead, we place very weak constraints on the parameters when the backward running filter is started. These constraints should be weak enough not to affect the parameter estimates but no so weak as to cause significant rounding error in the computations. The constraint which we have found works well in practice is to start the backward filter with *apriori* variances which are one thousand times greater than the variances of the estimates of the parameters at the end of the forward filter run. This weak constraint should change the smoothed estimates of the parameters by about one thousandth of their standard deviation (see discussion below).

The Kalman filter equations given in Equations (A.1)–(A.18) are relatively easy to implement in a computer program. However, there are items about, and some special forms of, these equations which are worth noting. The two items which we will discuss are the effects of *a priori* constraints placed on the parameters, and the implementation of white noise stochastic process. The Kalman filter equations are formulated such that the covariance matrix of the parameters is manipulated as observations are input to the filter. Consequently, we need to start the filter with the covariance matrix of the *a priori* estimates of the parameters. In many applications we would like to start the filter with no constraints placed on the parameters at all. However, in a computer this option is not possible, *i.e.,* infinity cannot be truly represented. In addition, if we look at Equation (A.15), placing large *a priori* constraints will introduce large rounding errors into the processing since the final covariance matrix is obtained by decrementing $\mathbf{C}_{t+1}^t$ as each new set of observations is added to the filter. Given these considerations, it is worthwhile to consider how the *a priori* covariances affect the final estimates of the parameters and their covariance matrix. Since any *a priori* constraint can be treated as a set of observations, we will use the Kalman

filter equations to investigate the effects of the constraints. For the constraints, the partial derivative matrix $\mathbf{A_t}$ is simply a unit matrix, and the Kalman gain when the constraints are applied will be given by,

$$\mathbf{K} = \mathbf{C_t^t}(\mathbf{C_0} + \mathbf{C_t^t})^{-1} \tag{A.20}$$

where $\mathbf{C_0}$ is the matrix of *a priori* variances, and $\mathbf{C_t^t}$ is the covariance matrix of the parameter estimates without the constraint applied. If we use the matrix identity that $(\mathbf{A} + \mathbf{B})^{-1} = \mathbf{B}^{-1}(\mathbf{A}\mathbf{B}^{-1} + \mathbf{I})^{-1}$, where $\mathbf{I}$ is a unit matrix, then $\mathbf{K}$ reduces to,

$$\mathbf{K} = \left(\mathbf{C_0}(\mathbf{C_t^t})^{-1} + \mathbf{I}\right)^{-1} \tag{A.21}$$

and the estimates of the parameters with the constraint applied becomes

$$\hat{x} = \hat{x}_t^t + \left[\mathbf{C_0}(\mathbf{C_t^t})^{-1} + \mathbf{I}\right]^{-1}(x_0 - \hat{x}_t^t) \tag{A.22}$$

where x_0 is a vector of *a priori* values. In general Equation (A.22) is difficult to solve analytically. However, we can treat the special case when $\mathbf{C_t^t}$ is a diagonal matrix. (We also assume that $\mathbf{C_0}$ is a diagonal matrix.) Denoting the diagonal elements of $\mathbf{C_0}$ and $\mathbf{C_t^t}$ for the ith parameter by σ_{0i}^2 and σ_{ti}^2, respectively, the change in the estimate of the ith parmeter when the constraint is applied is given by

$$\Delta x_i = \frac{\sigma_i^2}{\sigma_0^2}(x_{0i} - x_{ti}^t) \tag{A.23}$$

where we have assumed that $\frac{\sigma_i^2}{\sigma_0^2} \ll 1$. From Equation (A.23) we see that the change in the parameter estimate due to the constraint being applied is the adjustment to parameter value by the ratio of the *a posterori* variance to the *a priori* variance. Similarly, it may be shown the change in the estimate of the variance of the parameters is also given by $\frac{\sigma_i^2}{\sigma_0^2}$. Another case which can be easily studied is when all of the parameters are highly correlated. In this case, the effect of the constraint is n times greater than in the uncorrelated case, where n is the number of highly correlated parameters. We have found that these simple rules work well for any $\mathbf{C_t^t}$ encountered in our processing.

The special form of the Kalman filter equations which we wish to study is the case of white noise stochastic processes. For this type of process the part of the state transition matrix for the white noise process is zero. We will also assume the white

noise process is uncorrelated with any of the other noise in the system. We will now rewrite the Kalman filter equations in partitioned form. Equation (A.1) becomes

$$y_t = \begin{pmatrix} \mathbf{A}_t & \mathbf{A'}_t \end{pmatrix} \begin{pmatrix} x_t \\ n_t \end{pmatrix} + v_t \qquad (A.24)$$

where n_t is the vector of parameters in the white noise process, and $\mathbf{A'}_t$ is the matrix relating n_t to y_t. The other quantities in Equation (A.23) have the same meaning as before. The state transition Equation (A.2) becomes

$$\begin{pmatrix} x_{t+1} \\ n_{t+1} \end{pmatrix} = \begin{pmatrix} \mathbf{S}_t & 0 \\ 0 & 0 \end{pmatrix} \begin{pmatrix} x_t \\ n_t \end{pmatrix} + \begin{pmatrix} w_t \\ n_{t+1} \end{pmatrix}. \qquad (A.25)$$

The application of the Kalman filter equations to this type of system is straight forward. The prediction step for the parameters and their covariance matrix is given by (from Equations (A.12) and (A.13))

$$\begin{pmatrix} \hat{x}^t_{t+1} \\ \hat{n}^t_{t+1} \end{pmatrix} = \begin{pmatrix} \mathbf{S}_t & 0 \\ 0 & 0 \end{pmatrix} \begin{pmatrix} \hat{x}^t_t \\ \hat{n}^t_t \end{pmatrix} \qquad (A.26)$$

$$\begin{pmatrix} \mathbf{C}^t_{t+1} & 0 \\ 0 & \mathbf{C'}^t_{t+1} \end{pmatrix} = \begin{pmatrix} \mathbf{S}_t \mathbf{C}^t_t \mathbf{S}^{\mathbf{T}}_t & 0 \\ 0 & 0 \end{pmatrix} + \begin{pmatrix} \mathbf{W}_t & 0 \\ 0 & \mathbf{N}_t \end{pmatrix}$$

$$= \begin{pmatrix} \mathbf{S}_t \mathbf{C}^t_t \mathbf{S}^{\mathbf{T}}_t + \mathbf{W}_t & 0 \\ 0 & \mathbf{N}_t \end{pmatrix} \qquad (A.27)$$

where $\mathbf{C'}^t_{t+1}$ is the submatrix of covariance matrix for the white noise process. It should be noticed that this submatrix is simply $\mathbf{N}_t$. The Kalman gain for this system reduces to

$$\begin{pmatrix} \mathbf{K} \\ \mathbf{K'} \end{pmatrix} = \begin{pmatrix} \mathbf{C}^t_{t+1} \mathbf{A}_t \\ \mathbf{N}_t \mathbf{A'}_t \end{pmatrix} \left(\mathbf{Q}_t + \mathbf{A'}_t \mathbf{N}_t \mathbf{A'}^{\mathbf{T}}_t + \mathbf{A}_t \mathbf{C}^t_{t+1} \mathbf{A}^{\mathbf{T}}_t \right)^{-1} \qquad (A.28)$$

where $\mathbf{K'}$ is the submatrix of the Kalman filter gain for the white noise process. If we examine the expression for the Kalman gain of the non-white noise process parameters in Equation (A.28) we notice that the same expression for the Kalman gain would have been generated had we not explicitly included the white noise process parameters in the filter, but had instead simply modified the covariance matrix of the observations to include the effects of the white noise process i.e. $\mathbf{Q}_t + \mathbf{A'}_t \mathbf{N}_t \mathbf{A'}^{\mathbf{T}}_t$ would be substituted for $\mathbf{Q}_t$. This modification is valid for the remaining equations in the Kalman filter as

well. We have found this procedure useful whenever white noise processes are needed in the Kalman filter since it reduces the number of parameters which need to be explicitly included in the filter.

A very useful application for the above procedure occurs when both delay and rate data are included in the filter, and a random walk (for delays) is included in the stochastic models. For the rate data, this random walk process will manifest itself as white noise. If the duration of the observations is short compared to time interval between the observations, then the white noise at the "instant" of observation will be independent of the integrated effect of the white noise sensed by the delay data. Thus, the effects of the random walk on the rate data can be included using the procedure given above. However, in practice, the duration of the observations is not short compared to interval time between measurements and thus the procedure given about is not valid. We will defer furthur discussion of this topic until we discuss the effects of the finite of duration of observations on modeling stochastic processes in Appendix B.

Appendix B. Properties of stochastic processes

Here we discuss the properties of the stochastic processes we have used in out implementation of the Kalman filter. We will firstly define each of the statistical characterizations given in Table A.1; then we will discuss the derivations of some of these characterizations; and finally we will discuss the effects of averaging the stochastic processes. For each of the stochastic processes we give the following. *(i) Driving differential equation.* In all cases the process is assumed to be driven by white noise, $w(t)$. *(ii) Solution.* This expression is the solution to the differential equation which drives the process. *(iii) covariance function,* $R(t_1,t_2)$. The covariance function is defined as,

$$R(t_1,t_2) = \langle p(t_1)p(t_2)\rangle \qquad (B.1)$$

where $p(t)$ is the value of the process at time t, and $\langle\rangle$ denotes the expectation value. When the covariance function depends only on t_1-t_2, the function is stationary, and the covariance function is expressed in terms of τ=t_1-t_2. *(iv) Power spectral density function (PSD),* $S(f)$. For stationary stochastic processes, the PSD is defined as,

$$S(f) = \int_{\infty}^{\infty} R(\tau)e^{-\imath 2\pi f\tau}d\tau \qquad (B.2)$$

where f is frequency in cycles per unit time. *(v) 2-sample Allan variance, $\sigma_y^2(\tau)$.* The 2–sample Allan variance is defined by (Vessot, 1976),

$$\sigma_y^2(\tau) = \langle p^2(t+\tau) - 2p(t+\tau)p(t) + p^2(t)\rangle/\tau^2 \qquad (B.3)$$

where the expectation is taken over all times t. For all of the stochastic processes given in Table A.1, $\sigma_y^2(\tau)$ is only a function of τ, the time interval between samples, and not the time at which the samples are taken. The form of the 2–sample Allan variance is such that the results are independent of any mean value or mean slope in the values of $p(t)$. This property is particularly advantageous to the study of hydrogen maser clocks because their absolute frequency is often not well controlled. Also, we refer to the Allan standard deviation most of the time which we define to be the square–root of the 2–sample Allan variance. *(vi) Structure function, $D(t,\tau)$.* The structure function, which is often used in atmospheric studies, is defined as

$$D(t,\tau) = \langle \big(p(t+\tau) - p(t)\big)^2 \rangle. \qquad (B.4)$$

where the expectation is taken over all times t. As for the Allan variance, the structure function may depend on t as well as τ.

The derivations of the entries given in Table A.1 are tedious but straightforward given the solutions to the differential equations for each stochastic process. For each of the processes, Φ_α (where α is w for the white noise, r for the random walk, i for the integrated random walk, and g for the first–order Gauss Markov processes) is the PSD of the white noise driving the process. The variance of the driving white noise is $\Phi_\alpha\delta(0)$ where $\delta(0)$ is the Dirac delta function *i.e.*, $\langle w(t)w(t+\tau)\rangle = \Phi_\alpha\delta(\tau)$.

Some general comments can be made about the nature of the processes given in Table A.1. For the random walk and the integrated random walk the PSD functions are not defined because neither of these processes is stationary, *i.e.*, their variances tend to infinity as time tends to infinity. In our application this property does not pose a major problem because we only need the stochastic model to predict the variance of the change in the process over the interval of time between observations. An interval which is typically less than 1000 seconds. When there are large gaps in the VLBI data (>1000 seconds), the random walk and integrated random walk models tend to overestimate the variance of the changes in the processes. The net effect is that

information about the change in the process values over the gap will come more from the VLBI data themselves than from the prediction based on the stochastic model.

In our implementation of the Kalman filter the random walk process is the one most often used. This process seems appropriate for representing the short period fluctuations ($< 10^4$ seconds) of the clocks and the fluctuations of the atmospheric delays. Since the changes in the values of the random walk processes over the duration of a VLBI observation are not small, we will consider in detail the incorporation of this stochastic process in the filter. We consider two VLBI observations of durations Δ_1 and Δ_2 with the centers of the observations at times t_1 and t_2. The estimates of the values of VLBI delay and rate observables averaged over the two durations is

$$\tau_i = \int_{t_i-\Delta_i}^{t_i+\Delta_i} p(u)du/2\Delta_i \qquad (B.5)$$

$$\dot{\tau}_i = \frac{3}{2\Delta^3}\int_{t_i-\Delta_i}^{t_i+\Delta_i} (u-t_i)p(u)du \qquad (B.6)$$

where i is either 1 or 2 denoting the first or second observation. Given these expressions for the delay and rate, we can subsitute the equations for the random walk process noise (from Table A.1), and evaluate the statistical properties of the averages. The following expressions can be derived for the statistical properties of the delays and rates at the two times:

$$\langle \tau_i^2 \rangle = \Phi_r t_i - \Phi_r \Delta_i/6 \qquad (B.7)$$

$$\langle \dot{\tau}_i^2 \rangle = \frac{6\Phi_r}{5\Delta_i} \qquad (B.8)$$

$$\langle \tau_i \dot{\tau}_i \rangle = \Phi_r/2 \qquad (B.9)$$

$$\langle \tau_1 \tau_2 \rangle = \Phi_r t_1 \qquad \text{for } t_1 < t_2) \qquad (B.10)$$

$$\langle \dot{\tau}_1 \dot{\tau}_2 \rangle = 0 \qquad (B.11)$$

$$\langle \dot{\tau}_1 \tau_2 \rangle = \Phi_r. \qquad (B.12)$$

Our implementation of the Kalman filter does not adhere exactly with these equations. We neglect the small decrease in the variance of $\langle \tau_i^2 \rangle$ due to the term $\Phi_r \Delta_i/6$ because the appropriate durations of the observations is not always known especially

for the VLBI data taken in the 1970's. Nor do we account for the small correlation $(5\Delta_i/\sqrt{12(t_i - \Delta_i/6)},\ t_i > \Delta_i/2)$ between the delay and rate observations at each epoch of observation. To rigorously include the effects of this correlation in the Kalman filter would require the introduction of an additional parameter for each random walk process. This parameter would represent the average rate of change of the random walk over the duration of an observation. The process would still be a white noise sequence, but the sequence would be correlated with the random walk sequence for the delays. Thus, the assumption used in deriving Equation (A.27) would not valid, and we could not simply incorporate the rate process into the rate data covariance matrix. We do not feel that this is a major problem in the Kalman filter implementation because we are neglecting a small amount of information about the rate data which should result in the Kalman filter yielding slightly larger variances for the estimated parameters. If in the future, the time interval between observations becomes very short compared to the duration of the observations, we may modify the Kalman filter implementation to incorporate the correlation between delay and rates. Also, at this time, we generate all of our geodetic results using only delay data. The neglected correlation has no impact at all on this type of solution. We adopt this procedure because including the rate into the geodetic solutions has a minimal effect on the estimates of the geodetic parameters and their variances.

TABLE A.1. Characteristics of some stochastic processes.

White noise, $p_w(t)$	Random Walk, $p_r(t)$
$p_w(t) = w(t)$	$\frac{dp_r(t)}{dt} = w(t)$
$p_w(t+\Delta t) = w(t+\Delta t)$	$p_r(t+\Delta t) = p_r(t) + \int_0^{\Delta t} w(u+t)du$
$R(\tau) = \Phi_w \delta(\tau)$	$R(t_1,t_2) = \Phi_r min(t_1,t_2)$
$S(f) = \Phi_w$	$S(f)$ not defined
$\sigma_y^2(\tau) = 3\Phi_w/\tau^2$	$\sigma_y^2(\tau) = \Phi_r/\tau$
$D(\tau) = 2\Phi_w \delta(0)$	$D(\tau) = \Phi_r \tau$
$p_w(t+\Delta t) = w(t+\Delta t)$	$p_r(t+\Delta t) = p_r(t) + \int_0^{\Delta t} w(u+t)du$

Integrated Random Walk, $p_i(t)$	First order Gauss Markov, $p_g(t)$
$\frac{d^2p_r(t)}{dt^2} = w(t)$	$\frac{dp_g(t)}{dt} = -p_g(t)\beta + w(t)$
$p_i(t+\Delta t) = p_i(t) + \Delta t \dot{p}_i(t) + \int_0^{\Delta t} (\Delta t - u) w(u+t)du$	$p_g(t+\Delta t) = e^{-\Delta t\beta} p_g(t) + e^{-\Delta t\beta} \int_0^{\Delta t} e^{u\beta} w(t+u)du$
$\dot{p}_i(t+\Delta t) = \dot{p}_i(t) + \int_0^{\Delta t} w(u+t)du$	
$R(t_1,t_2) = \Phi_i t_1^2 (3t_2 - t_1)/6$	$R(\tau) = \frac{\Phi_g}{2\beta} e^{-\lvert\tau\rvert\beta}$
$S(f)$ not defined	$S(f) = \frac{\Phi_g}{\beta^2(1+(2\pi f/\beta)^2)}$
$\sigma_y^2(\tau) = \Phi_i \tau/3$	$\sigma_y^2(\tau) = \frac{\Phi_i}{2\beta\tau^2}(3 - 4e^{-\lvert\tau\rvert\beta} + e^{-2\lvert\tau\rvert\beta})$
$D(t,\tau) = \Phi_i(\tau^3/3 + \tau^2 t)$	$D(\tau) = \frac{\Phi_g}{\beta}(1 - e^{-\lvert\tau\rvert\beta})$
$p_i(t+\Delta t) = p_i(t) + \Delta t \dot{p}_i(t) + \int_0^{\Delta t} (\Delta t - u) w(u+t)du$	$p_g(t+\Delta t) = e^{-\Delta t\beta} p_g(t) + e^{-\Delta t\beta} \int_0^{\Delta t} e^{u\beta} w(t+u)du$
$\dot{p}_i(t+\Delta t) = \dot{p}_i(t) + \int_0^{\Delta t} w(u+t)du$	

In each of the boxes we give the characteristics of the stochastic processes discussed in the text. The first item in each box is the driving differential equation for the process. The second entry is the solution to the differential equation for an arbitrary excitation function. $R(\tau)$ or $R(t_1,t_2)$ is the covariance function of the process, assuming that the excitation of function, $w(t)$, is white noise with a power-spectral density (PSD) of Φ_α where α is w for the white noise process, r

for the random walk, i for the integrated random walk, and g for the first–order Gauss Markov process. $S(f)$ is the PSD function where f is in cycles per unit time. $\sigma_y^2(\tau)$ is the 2–sample Allan variance at sampling time τ. $D(t,\tau)$ or $D(\tau)$ is the structure function for time interval τ. The final entry for each process is the solution to the driving differential equation for arbitrary excitation function $w(t)$. The definitions for each of these quantities and some discussion of the entries given in the table are given in Appendix B.

References

Davis, J.L., T.A.Herring, and I.I.Shapiro, Geodesy by radio interferometry: 1-2 part-per-billion precision for transcontinental baselines, to appear in *Proceedings of IAU Symposium No. 129, The Impact of VLBI on Astrophysics and Geophysics*, Eds. M.Reid, and J.M. Moran, Reidel, Dordrecht, 367–368, 1988.

Elgered, G., J.L. Davis, T.A.Herring, and I.I. Shapiro, Methods of correction for the "wet" atmosphere in estimating baseline lengths from VLBI, to appear in *Proceedings of IAU Symposium No. 129, The Impact of VLBI on Astrophysics and Geophysics*, Eds. M.Reid, and J.M. Moran, Reidel, Dordrecht, 543–544, 1988.

Elgered, G., J.L. Davis, T.A.Herring, and I.I. Shapiro, Geodesy by radio-interferometry: Water vapor radiometry for calibration of the wet delay, to be submitted to *J. Geophys. Res*, 1988

Gelb, A, *Applied optimal Estimation* MIT press, MIT, Cambridge, MA., pp 374, 1974.

Herring, T.A., C.R. Gwinn, B.A. Buffett, and I.I.Shapiro, Bound on the amplitude of the Earth's free core-nutation, *Proceedings of IAU Symposium No. 128, The Earth's rotation and Reference frame for geodesy and geodynamics*, A.K. Babcock and G.A. Wilkins (eds.), Reidel, Dordrecht, 293–299, 1988

Herring, T.A., VLBI studies on the nutations of the Earth, to appear in *Proceedings of IAU Symposium No. 129, The Impact of VLBI on Astrophysics and Geophysics*, Eds. M.Reid, and J.M. Moran, Reidel, Dordrecht, 371–376, 1988.

Liebelt, P.B., *An introduction to optimal estimation*, Addision-Wesley, pp 273, 1967.

Vessot, R.F.C, Frequency and time standards, in *Methods of experimental physics*, 12C, M.L. Meeks, Ed., Academic Press, New York, pp 198–227, 1976.

METHODS OF CORRECTION FOR THE "WET" ATMOSPHERE IN ESTIMATING BASELINE LENGTHS FROM VLBI

G. Elgered, J. L. Davis, T. A. Herring, and I. I. Shapiro
Center for Astrophysics
60 Garden Street
Cambridge, MA 02138

ABSTRACT. The error in VLBI estimates of baseline length caused by unmodelled variations in the propagation path through the atmosphere is greater for longer baselines. We present and discuss series of estimates of baseline lengths obtained using different methods to correct for the propagation delay caused by atmospheric water vapor. The main methods are use of data from a water-vapor radiometer (WVR) and Kalman-filtering of the VLBI data themselves to estimate the propagation delay. Since the longest timespan of WVR data associated with geodetic VLBI experiments was obtained at the Onsala Space Observatory in Sweden, we present results for the following three baselines: (1) Onsala–Wettzell, FRG (920 km), (2) Onsala–Haystack/Westford, MA (5600 km), and (3) Onsala–Owens Valley (7914 km).

1. INTRODUCTION

This paper addresses the utility of water-vapor radiometers (WVR) in geodetic radio-interferometry experiments. The WVR data are providing *a priori* information about the wet delay. It is also possible to estimate a correction to any *a priori* delay during post-processing. The estimate can be of a mean zenith bias for the entire experiment or of values of samples of, say an assumed random (Markov) process. We have analyzed 77 experiments (made during 1980–1985) several times, each time with a different method to correct for the wet delay at Onsala, but with the atmospheric delays for all other sites (as well as the clocks) modeled as Markov processes.

2. RESULTS AND DISCUSSION

The results are presented in Table I as weighted root-mean-square (WRMS) scatters of baseline lengths about estimated slopes. The WRMS value is a measure of repeatability. We also present one solution where observations made at elevation angles lower then 25° ($\epsilon < 25°$) at Onsala were deleted since low elevation angle observations are not important when no delay corrections are estimated (*Herring* 1986). The WRMS for the Wettzell–Onsala baseline is given with respect to its mean value since no baseline change is expected. For this baseline, when the WVR data are used in place of the Markov process, the WRMS decreases from 5.2 to 4.0 mm. If we assume that atmospheric delay errors are not correlated with other errors, and that the wet atmospheres over Wettzell and Onsala are statistically similar, the WRMS would be 2.2 mm were a WVR installed at Wettzell. The results for the Haystack/Westford–Onsala baseline are presented for each of the former antennas separately since the WRMS is significantly different in the two cases. This

TABLE I. BASELINE LENGTH REPEATABILITY

Baseline Onsala to	Method used to correct for the wet delay at Onsala		Mean baseline[5] +919660 m (mm)	WRMS about mean (mm)
	A priori	Adjustment		
Wettzell[1]	None	Offset	999 ± 1	5.8
Wettzell[1]	None	Markov	1000 ± 1	5.2
Wettzell[1]	WVR	Offset	999 ± 1	5.1
Wettzell[1]	WVR	None	996 ± 1	4.0
Wettzell[1]	WVR ($\epsilon > 25°$)	None	996 ± 1	4.4
			Slope[5] (mm/year)	WRMS about slope (mm)
Haystack[2]	None	Offset	17.8 ± 1.4	14.1
Haystack[2]	None	Markov	19.0 ± 1.2	12.8
Haystack[2]	WVR	Offset	16.1 ± 1.2	12.5
Haystack[2]	WVR	None	14.2 ± 1.5	15.0
Haystack[2]	WVR ($\epsilon > 25°$)	None	16.6 ± 1.1	11.5
Westford[3]	None	Offset	15.9 ± 2.5	21.6
Westford[3]	None	Markov	17.8 ± 2.1	18.3
Westford[3]	WVR	Offset	14.5 ± 2.5	21.8
Westford[3]	WVR	None	13.7 ± 2.8	23.1
Westford[3]	WVR ($\epsilon > 25°$)	None	15.8 ± 2.3	18.8
Owens Valley[4]	None	Offset	12.8 ± 4.0	39.1
Owens Valley[4]	None	Markov	12.7 ± 3.2	31.4
Owens Valley[4]	WVR	Offset	10.3 ± 3.2	31.3
Owens Valley[4]	WVR	None	9.0 ± 6.1	57.6
Owens Valley[4]	WVR ($\epsilon > 25°$)	None	11.4 ± 3.6	35.4

[1] 25 experiments [2] 36 experiments [3] 45 experiments [4] 29 experiments
[5] The sigmas are scaled so that reduced $\chi^2 = 1$ (*Herring et al.* 1986).

difference indicates that the accuracy of the Westford-Onsala baseline estimates is not limited by atmospheric errors. It is also clear that low elevation observations do not improve the accuracy of baseline length estimates when WVR data are used and no adjustment to the *a priori* delay is estimated. Finally, for the longest baseline (Owens Valley–Onsala) it appears better to estimate a correction to the zenith delay inferred from the WVR data rather than to discard low elevation observations, because a bias affects the accuracy of the vertical position which is more important for estimates of length of longer baselines.

3. CONCLUSIONS AND SUGGESTIONS FOR FUTURE WORK

The differences in the rates obtained with the different methods are small compared to 1 cm/year. It is important to minimize possible biases in the atmospheric delays inferred from WVR data. A main source of such bias is the uncertainty of the attenuation coefficients due to water vapor. Another important task is to find the "best" elevation cut-off angle when WVR data are to be used.

ACKNOWLEDGMENTS

This work was supported by the Air Force Geophysics Laboratory, contract F-19628-86-K-0025; NASA grant NAG5-538; and NSF grants EAR-83-06380 and EAR-86-18989.

REFERENCES

Herring, T.A., *J. Geophys. Res.*, 91, No. B9, pp. 9177–9182, 1986.
Herring, T.A. et al., *J. Geophys. Res.*, 91, No. B8, pp. 8341–8347, 1986.

Geodesy by radio-interferometry:

Water vapor radiometry for calibration of the wet delay

G. Elgered, J. L. Davis, T. A. Herring, and I. I. Shapiro

Harvard-Smithsonian Center for Astrophysics

60 Garden Street

Cambridge, MA 02138

To be submitted to

J. Geophs. Res, 1988

ABSTRACT

An important source of error in very-long-baseline interferometry (VLBI) estimates of baseline length is unmodeled variations of the refractivity along the propagation path through the atmosphere. We present and discuss the method of using data from a water-vapor radiometer (WVR) to correct for the propagation delay caused by atmospheric water vapor. Data from different WVR's are compared with estimated propagation delays obtained by Kalman-filtering of the VLBI data themselves. The consequenses of using either WVR data or Kalman filtering to correct for atmospheric delays at the Onsala VLBI site are investigated by studying the repeatability of estimated baseline lengths from Onsala to several other sites. The lengths of the baselines ranges from 919 to 7941 km. The repeatability obtained for baseline-length estimates show that the methods of water-vapor radiometry and Kalman filtering offer comparable accuracies when applied to the climate of the Swedish west coast. It is also clear that observations made at low elevation angles should not be used at a site where WVR data are available if no estimations of the atmospheric delay is made for that site from the interferometer data. The actual "best" cut-off in elevation angle depends on the accuracy of the total delay since its error increase with increasing air mass. In this study the best cut-off is found to be about 20° when WVR data are used.

INTRODUCTION

To correct for the "wet" atmospheric delay, water-vapor radiometers (WVR's) have been developed for radio-interferometry experiments designed for estimation of geodetic parameters. This delay, although much smaller then the delay caused by the "dry" constituents of air, is—due to its variability in space and time—a major source of error in estimates of geodetic parameters such as baseline-lengths.

WVR data can be treated as *a priori* (*i.e.*, prior to least-squares estimation of site positions, etc.) information about the wet delay. Other *a priori* data are ground measurements of humidity and temperature that can be used with a model to predict the wet delay. Due to poor mixing of wet and dry air the accuracy of this type of model is expected to be too poor to be useful for our application. For comparison, however, we use a model of this type: *Saastamoinen's* [1972]; we will refer to it as the ground-based model.

It appears that there is no practical possibility other than use of a remote sensing instrument, such as the WVR, in connection with baseline-length estimation from very long-baseline-interferometry (VLBI) data. However, it is also possible to estimate a correction to any *a priori* delay together with geodetic and other parameters from the VLBI data. We can estimate a mean zenith bias for the entire experiment or values of samples of, say, an assumed random (Markov) process [*Herring et al.*, 1988] representing the delay.

This paper addresses the utility of water-vapor radiometers (WVR) in geodetic radio-interferometry experiments. First, a general background of atmospheric delays and water-vapor radiometry will be given. Thereafter, we describe the

different WVR's that have been used to collect the data now analyzed. The results are presented in two ways. First we compare the inferred wet delay variations from the WVR and the Kalman filter for several experiments. Second, we compare the repeatability of estimated baseline lengths obtained using different methods to correct for the atmospheric delays. Since the longest timespan of WVR data associated with geodetic VLBI experiments was obtained at the Onsala Space Observatory in Sweden, we present series of estimates of lengths from Onsala to Wettzell, FRG; Haystack/Westford, MA; Richmond, FL; Owens Valley, CA; and Fort Davis, TX.

THE ATMOSPHERIC DELAY AND WATER VAPOR RADIOMETRY

The delay through the neutral atmosphere depends on two terms (*Davis et al.*, 1985). The first is called the "hydrostatic" (or dry) delay. Its value ΔL_h in the zenith direction, expressed in meter is

$$\Delta L_h = (0.0022768 \pm 0.0000015)\,\frac{P_o}{f(\Phi, H)} \tag{1}$$

where P_o is the total pressure at the ground in mbar and where

$$f(\Phi, H) = (1 - 0.00266\cos 2\Phi - 0.00028H) \tag{2}$$

is used to model the variation of the acceleration due to gravity with latitude Φ and the height of the station H, in km, above the geoid. The uncertainty given for the hydrostatic delay is the root sum square of the uncertainties in the measurements

of the refractivity, the acceleration due to gravity, the universal gas constant, and the variability of the dry mean molar mass, but not in any departures from hydrostatic equlibrium.

The elevation dependence of the hydrostatic delay is modeled by using a "mapping function" whose accuracy is improved if other meteorological measurements, such as of the ground temperatures, are used (see *e.g.*, *Hopfield* [1971]). The mapping function used for the hydrostatic delay in this study is presented by *Davis et al.* [1985].

The second term of the total delay is the wet delay, ΔL_w, which, defined consistently with the hydrostatic delay, can be written as

$$\Delta L_w = 10^{-6}\left[17\int_0^\infty \frac{e}{T}\,ds + 3.776\times 10^5\int_0^\infty \frac{e}{T^2}\,ds\right] \qquad (3)$$

expressed in the same units as is the path, s; T is the temperature in K; and e is the partial pressure of water vapor in mbar. This wet delay is determined mainly by the amount of water vapor along the atmospheric path.

The WVR measures the emission from the sky at two (or more) well separated frequency bands near the water-vapor emission line centered between 22 and 23 GHz. The WVR intensity output, for the band closest to the center of this line will depend mainly on the amount of water vapor in the direction the WVR antenna is pointed. A second frequency band is needed to correct for emission caused by liquid water, which occasionally can be larger than the vapor contribution (even at the center of the water-vapor line). Using the Rayleigh-Jeans

approximation and the equation of radiative transfer [*Chandrasekar*, 1950], we can write the sky-brightness temperature measured by the WVR as

$$T_s = T_{bg} e^{-\tau_\infty} + \int_0^\infty T(s)\, \alpha(s)\, e^{-\tau(s)}\, ds \tag{4}$$

where T_{bg} is the "background" radiation (*i.e.*, from outside the earth's atmosphere). In the frequency band relevant to WVR's T_{bg} is due to the cosmic background radiation. $T(s)$ is the physical temperature along the path and $\alpha(s)$ is the attenuation coefficient due to water vapor, liquid water and oxygen. The parameter $\tau(s)$ is the corresponding opacity from the ground to the point s:

$$\tau(s) = \int_0^s \alpha(s')\, ds' \tag{5}$$

When s is equal to infinity the opacity is written as τ_∞. Each of the attenuation coefficients has its own frequency dependence which makes it possible to separate approximately the effects due to oxygen, water vapor, and liquid water.

When studying (3)–(5) it becomes clear that by making some approximations we can formulate several (non-unique) algorithms which will allow us to estimate the wet delay from WVR measurements of sky-brightness temperature. It is possible to take many different approaches. Empirical parameters in the algorithm show dependence on meteorological conditions such as vertical profiles of temperature in the atmosphere. Algorithms can therefore be optimized to a particular site. Different wet delay algorithms have been derived by *Resch* [1983], *Gary et al.* [1985], *Johansson et al.* [1987], and *Robinson* [1988]. These algorithms are

derived for many VLBI sites used (or to be used) in geodetic experiments and most of them make use of meteorological parameters measured at the ground.

Let us define the "algorithm error" as the error of the wet delay inferred from noise free radiometer observables. The algorithm error can then be divided into two parts. The first part is a scatter which varies on time scales of hours or longer. We obtain this error if we assume that the expressions for radio signal attenuation used to derive the algorithm are correct. For the algorithms referred to above, the root-mean-square (RMS) error of this part, for the zenith direction, varies between 0.1 to 0.4 cm, depending on algorithm and site, for weather situations excluding rain or heavy rain-clouds. The second part of the algorithm error, due to uncertainties in the attenuation coefficients, is believed to be more of a bias error over time scales of a day, the typical length of a geodetic VLBI experiment.

The uncertainty in the attenuation of oxygen is the least important and corresponds to an uncertainty in the inferred delay in the zenith direction of less than 2 mm. This value is derived by comparing the results from using different attenuation coefficients for oxygen [*Meeks and Lilley*, 1963; *Snider and Westwater*, 1969; *Liebe*, 1985; *Liebe*, 1987; *Rosenkranz*, 1987] in the algorithm.

The attenuation due to liquid water is assumed to be proportional to the square of the frequency. This frequency dependence is valid as long as the size of the liquid water drops are much smaller than the wavelength of the attenuated signal [*Staelin* 1966]. For all the WVR's used for geodetic VLBI, the "cloud correction band" has the highest frequency and is centered at about 31 GHz (wavelength $\approx$ 1 cm). If the size of the drops in the atmosphere become comparable to the

wavelength (say a few tenths of a mm) the algorithm will overestimate the wet delay [*Westwater* 1972]. An example of the effect of large drops is given in Figure 1, where the effect is further increased by the accumulation of water drops on the teflon-covers of the horn antennas. During the rain, the WVR data are then of no use for the calculation of accurate delay corrections.

The uncertainty in the attenuation due to water-vapor is the most important factor. The present uncertainties of these formulas are about 4 to 8%, with the uncertainty increasing with decreasing temperature [*Elgered* 1989]. These uncertainties are obtained by using different expressions for the attenuation coefficients in the derivation of the algorithm [*Staelin* 1966, *Waters* 1976, *Liebe* 1985, *Liebe* 1987]. Even a 4% error is, however, not negligible. Zenith wet delays of between 10 cm and 30 cm are not unusual in the temperate summer. For a typical elevation angles of 30°, we will then obtain errors of the order of 1–3 cm in our estimated delay corrections. These errors are large when compared to the uncertainties of VLBI group delay observations which are 1 cm or less.

BRIEF DESCRIPTION OF WATER-VAPOR RADIOMETERS

Design and manufacturing of WVR's specifically for use in geodetic VLBI experiments started in the mid seventies at the Jet Propulsion Laboratory (JPL) in Pasadena, CA, where seven WVR's were built [*Resch et al.* 1985] and at the Onsala Space Observatory in Sweden where one WVR was built [*Elgered and Lundh* 1983]. Later four of the JPL instruments (known as R-series WVR's) were upgraded and

a new more compact WVR was made at JPL (J-series WVR) [*Janssen* 1985]. More J-series WVR's are now being built and another, independently designed, WVR is being built at the Geodetic Institute in Bonn for the VLBI station in Wettzell, FRG.

The different WVR's that have been used in Mark-III VLBI experiments are briefly described in Table 1. System noise-temperatures are all about 600 K. The WVR's are all fully steerable in azimuth and elevation, but the slew speeds are quite different. Even though all antennas used for VLBI observations typically slew at 0.5–2°/s, it is an advantage to have a higher slewing speed for the WVR. Instrumental calibrations are generally formulated as corrections to reference loads or noise-diodes and obtained by frequently performing elevation scans (also known as "tip-curves"). This procedure should be more successful if the WVR slews faster than the VLBI antenna thus allowing time between the VLBI observations for tip-curves.

The tip-curve method is sensitive to any inhomogeneities in the atmosphere; but, provided that tip-curves are carried out at diffrent azimuth angles, even simple gradients are easily detected and modeled. If the atmosphere is very inhomogeneous, which is often the case when significant amounts of liquid water are present, the noise in the tip-curve data becomes very apparent and the data can be downweighted before using them in the calibration procedure.

WET DELAYS INFERRED FROM WVR DATA AND FROM THE KALMAN FILTER

When the Kalman filter is used to estimate the atmospheric delay [*Herring et al.*, 1988], the normal procedure is to use the measured ground pressure to calculate the hydrostatic delay using (1) and (2), and to estimate an additional delay which is then assumed to be equal to the wet delay. The estimated wet delay using the Kalman-filter will, therefore, have an additional uncertainty arising from errors in the *a priori* estimates of the hydrostatic delay. Since the water vapor has a different distribution with height than has the dry air, a special "wet mapping function" has to be used to calculate the partial derivatives in the estimation process. We have used the mapping function presented by *Chao* [1972] for the elevation dependence of the wet delay.

When comparing the two methods, one limitation is the unavailability of WVR data at all sites and times. Figures 2–4 show the equivalent zenith wet delay inferred from WVR data and estimated from the VLBI data themselves, using the Kalman filtering technique. The data are from different sites and involve different WVRs. We have omitted the errorbars for the WVR data which vary between 5 and 8 mm for the old R-series WVR and between 2 and 4 mm for the other instruments. The variations for a given instrument are mainly determined by the elevation angle of the observation. In addition to these errors, there are biases in the measurements and in the inversion algorithm which have to be included.

In Figure 2 the WVR data are from the old R-series used at the Haystack observatory, MA; Figure 3 shows the same type of comparison for the Mojave

site, located in the Mojave desert in California. Figure 4 shows one of the best agreements obtained. It consists of three contiguous experiments: a 24 hour long "Cross-Atlantic" experiment including Westford, Onsala, and Wettzell; a 24 hour long "IRIS"one, including Westford, Fort Davis, Richmond, Onsala, and Wettzell; and a 30 hour long "Polar" experiment including Kashima, Fairbanks, Mojave, Westford, Onsala, and Wettzell. The Cross-Atlantic and Polar experiments are planned and scheduled within NASA's Crustal Dynamics Project and the IRIS experiment by the National Geodetic Survey.

It is of course possible to modify the parameters defining the Markov process in order to reflect that the expected wet delay variations vary with season and, especially, that there are large climatological differences between VLBI sites [*Herring et al.* 1988].

ON THE ABSOLUTE ACCURACY OF THE TOTAL DELAY

The comparisons shown in Figures 2-4 often exhibit similar short-term variations for the wet delay, but with a long-term bias evident. We have studied these biases for the Onsala site using a set of 101 Mark-III VLBI experiments in which WVR and VLBI data are both available at the Onsala site for more than approximately half of each experiment. These experiments were carried out from July 1980 to June 1987. The WVR data were used with the algorithm presented by *Johansson et al.* [1987] to estimate the wet delay. We used ground pressure measurements together with the WVR data to determine the *a priori* atmospheric

delay at Onsala, but allowed for an estimate of a constant correction to the equivalent delay in the zenith direction for each experiment. At all other sites the atmospheric delays were estimated by assuming the random behaviour could be represented by an integrated random walk process. The clocks at all sites were estimated assuming a random walk. The statistical parameters of the Markov process for the atmospheric delay estimation were obtained from previous analyses of the delay-rate residuals for each experiment [*Herring et al.*, 1988]. Ideally each estimate of this additional delay in the zenith direction would be zero. There are several sources of error which will influence the result:

1. Error in the inversion algorithm used with the WVR data, due to approximations of the atmospheric profiles of pressure, temperature, and humidity (2 mm RMS in the zenith direction for the algorithm used in this data set).

2. Error in the inversion algorithm used with the WVR data due to uncertainties in the attenuation coefficients of water vapor (approximately 4–8% of the wet delay).

3. WVR instrumental error (RMS scatter 3 mm, bias perhaps up to 1 cm).

4. Uncertainty of the wet refractivity (the constants in eq. (3), RMS 1% of the wet delay).

5. Error in the total pressure measurement (estimated peak-peak error at Onsala: $\pm$ 1 mbar, corresponding to $\pm$ 2.3 mm in equivalent zenith delay).

6. Uncertainty in equation (1) for the hydrostatic delay (RMS 0.1%, corresponding to 2.3 mm in equivalent zenith delay).

7. Violation of hydrostatic equilbrium in the atmosphere. Such errors should, however, only be important (larger than 1 mm in equivalent zenith delay) when strong winds exist. In this data set, there are no data taken at Onsala before March 1987 when the wind has exceeded 13 m/s due to a wind-speed limit for antenna operation.

8. Any unmodeled effect in the VLBI data which is absorbed in the atmospheric delay estimation such as errors in the mapping function used to estimate equivalent zenith delays; these are mainly sensitive to observations made at low elevation angles.

Three sets of solutions are presented in Figure 5. Each solution uses a different elevation cut-off angle for the observations made at Onsala. The effect of an error in the mapping function is expected to be larger at low elevations, which should be reflected in the estimated mean bias. Of course the uncertainty of estimated zenith bias increases rapidly with increasing cut-off angle but it is not possible to explain the bias mainly with errors in the mapping-function.

Since most of the errors associated with the wet delay are relative errors they can not alone explain the results in Figure 5. Such errors would increase in the summer when the wet delay is large and decrease in the winter. However, an instrumental bias of the WVR could, at least partly, be responsible for the mean error of about 1 cm. The existence of an instrumental bias can be investigated by a side-by-side comparison using another WVR and such an experiment is planned at Onsala in the near future.

Another source of error that deserves comment is the uncertainty in the observed total ground pressure. The observed pressures at the Onsala site used in this data set have been compared to the results from other pressure sensors in the area and corrected, if necessary. Thereafter, the pressure was referred to the height above sea-level where the signals are received by the radio telescope. We believe this procedure has resulted in an accuracy of the ground-pressure measurements of about 1 mbar corresponding to an equivalent zenith delay uncertainty of about 2 mm. Therefore, an effect due to measurement errors of the ground pressure can not alone be responsible for the biases shown in Figure 5.

USING WVR DATA AND LOW ELEVATION ANGLE OBSERVATIONS

Low elevation angle observations are not important when delay corrections are not estimated (*Herring* 1986). Such observations will actually degrade the accuracy of the estimated parameters if a bias error is present in the *a priori* delay.

Independent of the source of the bias discussed in the previous section, it is important to study the repeatability of estimated baseline lengths for different elevation cut-off angles when no atmospheric delays are estimated at the sites with WVRs. Some results are shown in Figure 6 where again the set of 101 experiments involving WVR data at Onsala are used. For each set of solutions made, for a given elevation cut-off angle, the weighted root-mean-square (WRMS) residuals of baseline lengths about the estimated slopes are presented. The WRMS value is

used as a measure of repeatability. There is a small improvement in repeatability for all baselines (excluding Onsala–Haystack) when we discard low elevation data. The effect is larger for the long baselines since the error made in the local vertical coordinate affects the baseline length more in these cases. The optimum cut-off angle is not identical for the different baselines. Since it is an advantage not to delete more data than necessary, a cut-off angle of 20° seems reasonable in all cases.

In order to show the effect more clearly, we have used the ground based model instead of the WVR data; the results are presented in Figure 7. The expected accuracy of this model, averaged over a year, is about 2 cm RMS in equivalent zenith delay for the Swedish west coast climate. In this case—since the expected bias during each experiment is larger—an elevation cut-off angle of about 30° is recommended. Note that the data deleted in this study are only those for observations made below the elevation angle cut-off at Onsala. If the cut-off criteria had been applied at other sites as well we would have had a much larger data loss (especially for the long baselines), implying a more rapid increase of the WRMS for higher cut-off angles.

RESULTS OF ESTIMATED BASELINE LENGTH REPEATABILITIES

The set of 101 experiments was analyzed several more times, each time with a different method used to correct for the wet delay at Onsala, but with the

atmospheric delays for all other sites (as well as the clocks for all sites) modeled as Markov processes.

The estimated slopes of the baselines from these analyzes are presented in Table 2 as all the WRMS scatters about these slopes. Based on the results presented in Figures 6 and 7 an elevation cut-off angle was applied when either WVR data or the ground-based model was used, and no estimates were made for the atmospheric delay at Onsala. The obtained repeatability is about the same in all cases which involve either the use of WVR data as *a priori* information or the estimation of the atmospheric delays based on their being Markov processes. The estimated rates of change of the baseline lengths are internally consistent, given their uncertainties, for all methods excluding that using the ground based model with no further estimation being made of the delay at Onsala. For two baselines (Onsala–Haystack and Onsala–Owens Valley) it appears better to estimate a correction to the zenith delay inferred from the WVR data than to discard low elevation observations. In the case of Haystack we know from Figure 6 that the low elevation data actually yielded a lower WRMS, even with no atmospheric bias being estimated. Note that the 90% confidence intervals are relatively large for these two baselines and that they have relatively more old data compared to the other baselines (see the mean time epochs given in Table 2). The WVR data, as well as the VLBI data, are believed to be least accurate in 1980.

The change of accuracy with time is further illustrated in Figure 8 where we have combined all the results from Onsala to Haystack and to Westford. The

WRMS for the last 18 experiments is 8 mm. when the WVR data are used, and 11 mm when instead, the delays are estimated.

CONCLUSIONS

The use of WVR data and the Kalman-filter for the "wet" delay calibration give comparable repeatability of estimated baseline lengths when used for the Onsala VLBI site. We find from our data set that the "best" elevation cut-off angle when WVR data are used is about 20°. Low elevation angles are, however, important since they imply a better geometry and are necessary to obtain accurate results if atmospheric delays are to be estimated [*Davis et al.* 1988]. Such estimates may be necessary if, for example, a WVR is not available at all sites or the WVRs may not be working properly at all sites. Even if a WVR is working properly, it may rain during a partion of an experiment, thus making the WVR data useless for our application. It is, therefore, of the greatest importance to minimize possible biases in the total atmospheric delay inferred from ground pressure and WVR data so that lower elevation angles can be used without degradation of the accuracy.

Most of the results in this paper involve WVR data taken with one specific instrument operating in the specific climate of the Swedish west coast. This WVR is not a state of the art instrument and the variations in the wet delay at Onsala are expected to be smaller than those present at many other geodetic VLBI sites. Therefore, a more accurate instrument at a more humid site should imply larger improvements when a WVR is used to correct for the wet delay.

Given the repeatability obtained using the Kalman-filter technique and the cost of a WVR, it may prove useful to have a WVR only at sites frequently used and/or where the expected wet delay variations are large. The WVR data can then also be used to check simultaneous Kalman filter estimates of the wet delay, to guard against other unmodeled errors in the VLBI data being absorbed into atmospheric delay estimates. The WVR is, over all, an excellent instrument for supplying continuous, accurate, and independent information on the wet delay in the atmosphere.

ACKNOWLEDGMENTS

This work was supported by the Air Force Geophysics Laboratory, contract F-19628-86-K-0025; NASA grant NAG5-538; and NSF grants EAR-83-06380 and EAR-86-18989.

REFERENCES

Chandrasekhar, S., *Radiative Transfer*, Oxford Univ. Press, New Jersey, 1950.

Chao, C.C., Private Communcation, 1972.

Davis, J.L., T.A. Herring, I.I. Shapiro, A.E.E. Rogers, and G. Elgered, Geodesy by Radio Interferometry: Effects of Atmospheric Modeling Errors on Estimates of Baseline Length, *Radio Science*, 20, pp. 1593–1607, 1985.

Davis, J.L., T.A. Herring, I.I. Shapiro, Geodesy by Radio Interferometry: Estimations of Relative Position Obtained from Transcontinental "Low Elevation-Angle" VLBI experiments, *J. of Geophys. Res.*, 1988, this volume.

Elgered, G. and P. Lundh, A Dual Channel Water Vapor Radiometer System, *Res. Rept. No. 145*, Chalmers University of Technology, Research Laboratory of Electronics and Onsala Space Observatory, 1983.

Elgered, G., Tropospheric Radio Path Delay from Ground-Based Microwave Radiometry, in *Atmospheric Remote Sensing by Microwave Radiometry*, ed. M. Janssen, Wiley & Sons, 1989.

Gary, B.L., S.J. Keihm, and M.A. Janssen, Optimum Strategies and Performance for the Remote Sensing of Path Delay Using Ground-Based Microwave Radiometers, *IEEE Trans. on Geoscience and Remote Sensing*, GE-23, pp. 479–484, 1985.

Herring, T.A., I.I. Shapiro, T.A. Clark, C. Ma, J.W. Ryan, B.R. Schupler, C.A. Knight, D.B. Schaffer, N.R. Vandenberg, H.F. Hinteregger, A.E.E. Rogers,

J.C. Webber, A.R. Whitney, G. Elgered, G. Lundqvist, B.O. Rönnäng, B.E. Corey, and J.L. Davis, Geodesy by Radio Interferometry: Evidence for Contemporary Plate Motion, *J. Geophys. Res.*, **91**, No. B8, pp. 8341-8347, 1986.

Herring, T.A., Precision of vertical position estimates from VLBI, *J. Geophys. Res.*, **91**, No. B9, pp. 9177-9182, 1986.

Herring, T.A., J.L. Davis, I.I. Shapiro, A Kalman Filter for the Analysis of Very-Long-Baseline Interferometric Data, *J. of Geophys. Res.*, 1988, this volume.

Hopfield, H.S., Tropospheric Effect on Electromagnetically Measured Range: Prediction from Surface Weather Data, *Radio Science*, 6, pp. 357-367, 1971.

Janssen, M.A., A New Instrument for the Determination of Radio Path Delay Variations due to Atmospheric Water Vapor, *IEEE Trans. on Geoscience and Remote Sensing*, GE-23, pp. 485-490, 1985.

Johansson, J.M., G. Elgered, and J.L. Davis, Geodesy by Radio Interferometry: Optimization of Wet Path Delay Algorithms Using Microwave Radiometer Data, *Res. Rept. No 152*, Onsala Space Observatory, Chalmers Univ. of Tech., 1987.

Liebe, H.J., An update model for millimeter wave propagation in moist air, *Radio Science*, 20, 1069–1089, 1985.

Liebe, H.J., A Contribution to Modeling Atmospheric Millimeter-wave Properties, *Frequenz*, 41, 31–36, 1987.

Meeks, M.L. and A.E. Lilley, The Microwave Spectrum of Oxygen in the Earth's Atmosphere, *J. Geophys. Res.*, 68, pp. 1683–1703, 1963.

Resch, G.M., M.C. Chavez, and N.I. Yamane, Description and Overview of an Instrument Designed to Measure Line-of-Sight Delay Due to Water Vapor, *TDA Progress Report 42-72*, Jet Propulsion Laboratory, Pasadena, California, pp. 1–19, 1982.

Resch, G.M., Inversion Algorithms for Water Vapor Radiometers Operating at 20.7 and 31.4 GHz, *TDA Progress Report 42-76*, Jet Propulsion Laboratory, Pasadena, California, pp. 12–26, 1983.

Resch, G.M., M.C. Chavez, N.I. Yamane, K.M. Barbier, R.C. Chandlee, Water Vapor Radiometry Research and Development Phase Final Report, *JPL Publication 85-14*, Jet Propulsion Laboratory, Pasadena, California, 1985.

Robinson, S.E., The Profile Algorithm for Microwave Delay Estimation From Water Vapor Radiometer Data, submitted for publication in *Radio Science*, 1988.

Rosenkranz, P.W., Interface Coefficients for Overlapping Oxygen Lines in Air, submitted to *J. of Quantitative Spectroscopy and Radiative Transfer*, 1987.

Saastamoinen, J., Atmospheric correction for the troposphere and stratosphere in radio ranging of satellites, in *The Use of Artificial Satellites for Geodesy, Geophys. Monogr. Ser.*, 15, edited by S.W. Henriksen *et al.*, pp. 247–251. American Geophysical Union, Washington, D.C., 1972.

Snider, J.B., E.R. Westwater. Atmospheric attenuation at 15, 31, and 53 GHz. *ESSA Tech. Report ERL 156-WPL 11*. U.S. Department of Commerce, Boulder, Colorado, 1969.

Staelin, D.H., Measurements and Interpretation of the Microwave Spectrum of Terrestrial Atmosphere near 1-Centimeter Wavelength, *J. of Geophys. Res.*, 71, pp. 2875–2881, 1966.

Waters, J.W., Absorption and Emission by Atmospheric Gases, in *Methods of Experimental Physics*, vol. 12B, edited by M.L. Meeks, Academic Press, New York, pp. 142–176, 1976.

Westwater, E.R., Microwave Emission From Clouds, *NOAA Technical Report ERL 219 - WPL 16*, U.S. Department of Commerce, National Oceanic and Atmospheric Administration, Environmental Research Laboratories, Boulder, CO., 1972.

TABLE 1. WATER-VAPOR RADIOMETERS
USED IN THE MARK-III VLBI EXPERIMENTS

	R-series[1]		New R-series[1]		J-series[1]			ASTRID[2]	
Frequencies [GHz]	20.7	31.4	20.7	31.4	20.7	22.2	31.4	21.0	31.4
Antenna beam-width [°]	7	7	7	7	9	9	7	6	6
Reference load temperatures [K]	313/413		313/413		313 + noise-diode			77/313 or 313/360[3]	
IF Bandwidth (DSB) [MHz]	5–100		10–110		40–200			5–500	
Slewing speed AZ,EL [°/s]	1.5, 1.5		7.5, 6.6		12, 60			1.7, 1.7	

[1] See text

[2] The WVR at the Onsala site (Atmospheric Sky Temperature Radiometer for Interferometric Delay corrections)

[3] Referred to as "cold" or "hot" mode. The WVR was running in hot mode during 6 of the 101 experiments analyzed in this study.

TABLE 2. BASELINE LENGTH REPEATABILITY

Baseline Onsala to	Method used to correct for the wet delay at Onsala[1]		Slope[2] (mm/year)		WRMS[3] about slope (mm)
	A priori	Adjustment			
Wettzell	None	Bias	-2.9±	0.9	5.7
(55 experiments,	None	Markov	-2.7±	0.6	4.2
919 km, mean	Model(30°)	None	-2.2±	0.9	5.8
epoch 1986.3)	Model	Bias	-2.6±	0.8	5.6
	Model	Markov	-2.6±	0.7	4.5
	WVR (20°)	None	-1.9±	0.6	4.2
	WVR	Bias	-2.3±	0.7	4.4
	WVR	Markov	-2.1±	0.7	4.4
Haystack	None	Bias	14.5±	1.3	14.1
(30 experiments,	None	Markov	15.2±	1.2	12.1
5600 km, mean	Model(30°)	None	14.3±	2.7	26.4
epoch 1984.0)	Model	Bias	12.0±	1.8	18.5
	Model	Markov	15.4±	1.2	11.3
	WVR (20°)	None	16.3±	1.3	13.3
	WVR	Bias	14.6±	1.2	11.5
	WVR	Markov	15.4±	1.3	12.0
Westford	None	Bias	13.4±	1.9	22.2
(78 experiments,	None	Markov	13.4±	1.3	14.2
5691 km, mean	Model(30°)	None	15.0±	2.1	24.0
epoch 1986.2)	Model	Bias	12.7±	1.8	20.5
	Model	Markov	13.2±	1.2	14.2
	WVR (20°)	None	12.7±	1.1	12.8
	WVR	Bias	13.8±	1.3	14.5
	WVR	Markov	14.2±	1.2	13.8
Richmond	None	Bias	0.5±	7.4	32.1
(24 experiments,	None	Markov	0.2±	5.6	24.9
7307 km, mean	Model(30°)	None	14.0±	9.3	39.7
epoch 1986.3)	Model	Bias	0.2±	6.1	26.7
	Model	Markov	0.6±	5.9	26.2
	WVR (20°)	None	4.3±	5.1	22.4
	WVR	Bias	6.3±	5.7	24.7
	WVR	Markov	6.4±	5.8	25.2
OVRO	None	Bias	16.9±	2.9	35.9
(27 experiments,	None	Markov	16.1±	2.6	30.4
7914 km, mean	Model(30°)	None	10.4±	3.4	40.2
epoch 1984.2)	Model	Bias	15.0±	2.4	29.7
	Model	Markov	15.9±	2.6	30.4
	WVR (20°)	None	17.7±	3.0	35.0
	WVR	Bias	15.2±	2.1	24.1
	WVR	Markov	16.6±	2.7	29.4

GRAS	None	Bias	14.4±	2.7	29.6
(64 experiments,	None	Markov	12.9±	1.8	25.3
7941 km, mean	Model(30°)	None	13.8±	2.6	36.3
epoch 1985.4)	Model	Bias	13.7±	2.4	30.4
	Model	Markov	12.9±	1.8	28.1
	WVR (20°)	None	13.8±	1.9	27.6
	WVR	Bias	12.9±	1.9	28.2
	WVR	Markov	13.6±	1.8	27.3

[1] The *a priori* information is none, or the ground-based model,or WVR. If an elevation cut-off angle is applied, its value is given in parantheses. If an atmospheric delay is estimated, it is assumed to be either a constant in the zenith direction (bias) or a Markov process.

[2] The sigmas are scaled so that reduced χ^2 per degree of freedom = 1 (*Herring et al.* 1986).

[3] weighted root-mean-square

FIGURE CAPTIONS

Figure 1

WVR mesurements carried out during four days in November 1986. The large errors in the inferred wet delays from WVR data taken during rain is in this case further increased by water-drops forming on the covers of the horn antennas. The errorbars for the WVR data have been omitted.

Figure 2

Simultaneous WVR measurements and Kalman filter estimates of the equivalent zenith wet delay at the Haystack Observatory. The old R-series WVR is used.

Figure 3

Simultaneous WVR measurements and Kalman filter estimates of the equivalent zenith wet delay at the Mojave VLBI site. The new R-series WVR is used.

Figure 4

Simultaneous WVR measurements and Kalman filter estimates of the equivalent zenith wet delay at the Onsala Space Observatory. The ASTRID WVR is used.

Figure 5

A constant atmospheric delay at Onsala estimated in the addition to an *a priori* delay consisting of the hydrostatic delay calculated using the total ground pressure and the wet delay inferred from WVR data. The estimation is done for 101 VLBI experiments three times, each time with a different elevation cut-off angle at Onsala in order to check the sensitivity of the estimated value for mapping function errors.

Figure 6

Weighted RMS residuals of estimated baseline lengths about a best fit straight line. The hydrostatic delay and WVR data are the *a priori* information used and no estimate of the atmospheric delay at Onsala is done. Eight sets of solutions are made, each one with a different elevation cut-off angle at Onsala. The baselines are from Onsala to: Wettzell (Z, 919 km, 55 experiments), Haystack (K, 5600 km, 30 experiments), Westford (E, 5601 km, 78 experiments), Richmond (R, 7307 km, 24 experiments), OVRO (O, 7914 km, 27 experiments), and GRAS (G, 7941 km, 64 experiments).

Figure 7

Weighted RMS residuals of estimated baseline lengths about a best fit straight line. The hydrostatic delay and the ground based model are the *a priori* information used and no estimate of the atmospheric delay at Onsala is done. For the explanation of the baselines see the caption to Figure 6.

Figure 8

Estimated baseline lengths from Onsala to the "combined" Haystack/Westford site. The circles denote measurements to Haystack and the triangles denote measurements to Westford. Either Haystack or Westford or both have been involved in all the 101 experiments studied. Since both sites have been involved in several experiments simultaneously there are 108 measurements all together. It is seen that both the formal error of the individual experiments and the repeatability have improved with time. The following milestones should be noted: June 1982: The Mark-III system is upgraded from 7 to 14 videoconverters implying better group delay measurements; May 1985: Westford installs cooled receiver and replaces Haystack in almost all CDP-experiments. August 1986: Onsala installs cooled receiver, and March 1987: Onsala installs a dual frequency feed in the 20m radome enclosed telescope which previously was used for the X-band only.

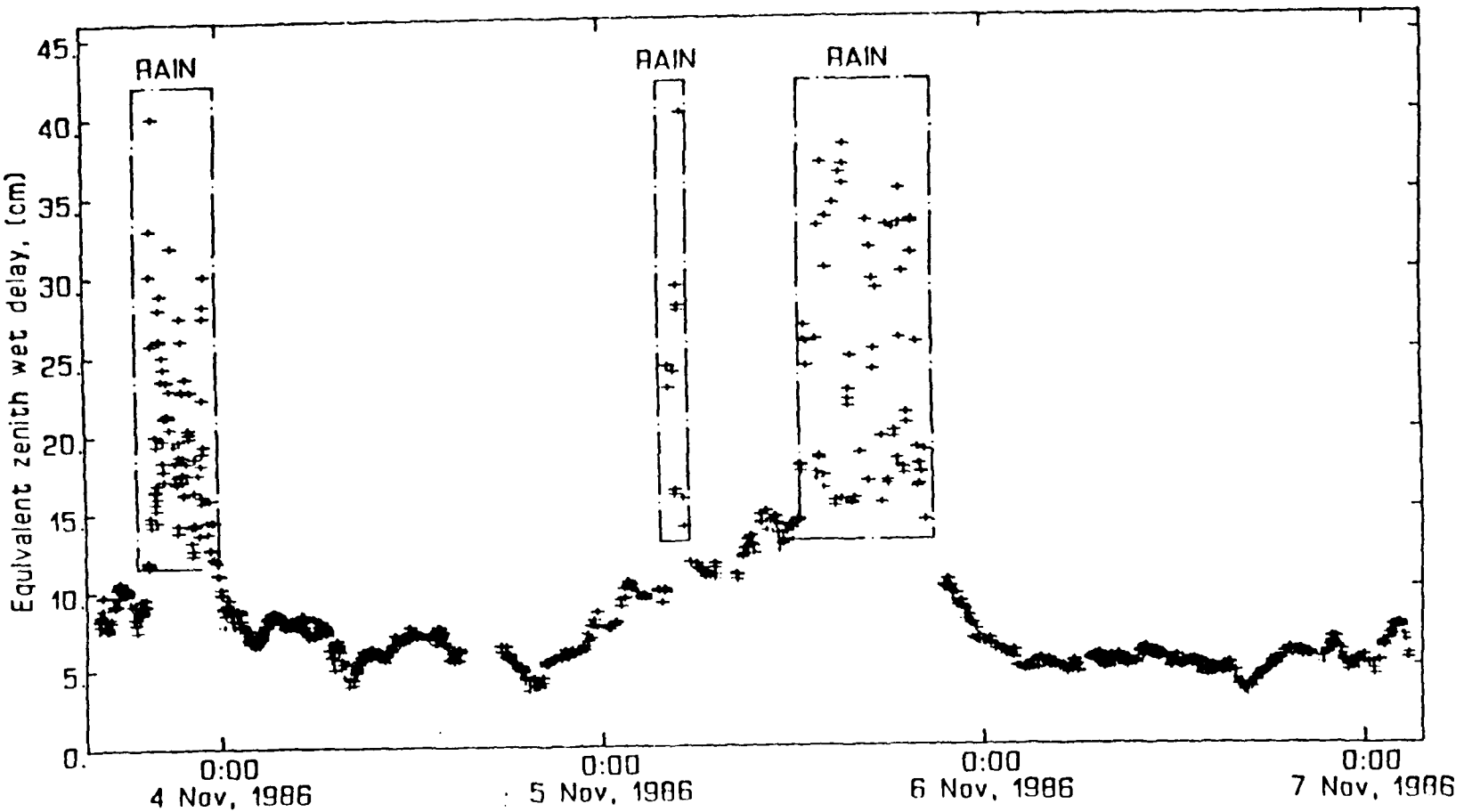
RAIN
RAIN
RAIN
Equivalent zenith wet delay, (cm)
45.
40.
35.
30.
25.
20.
15.
10.
5.
0.
0:00
4 Nov, 1986
0:00
5 Nov, 1986
0:00
6 Nov, 1986
0:00
7 Nov, 1986

FIGURE 1

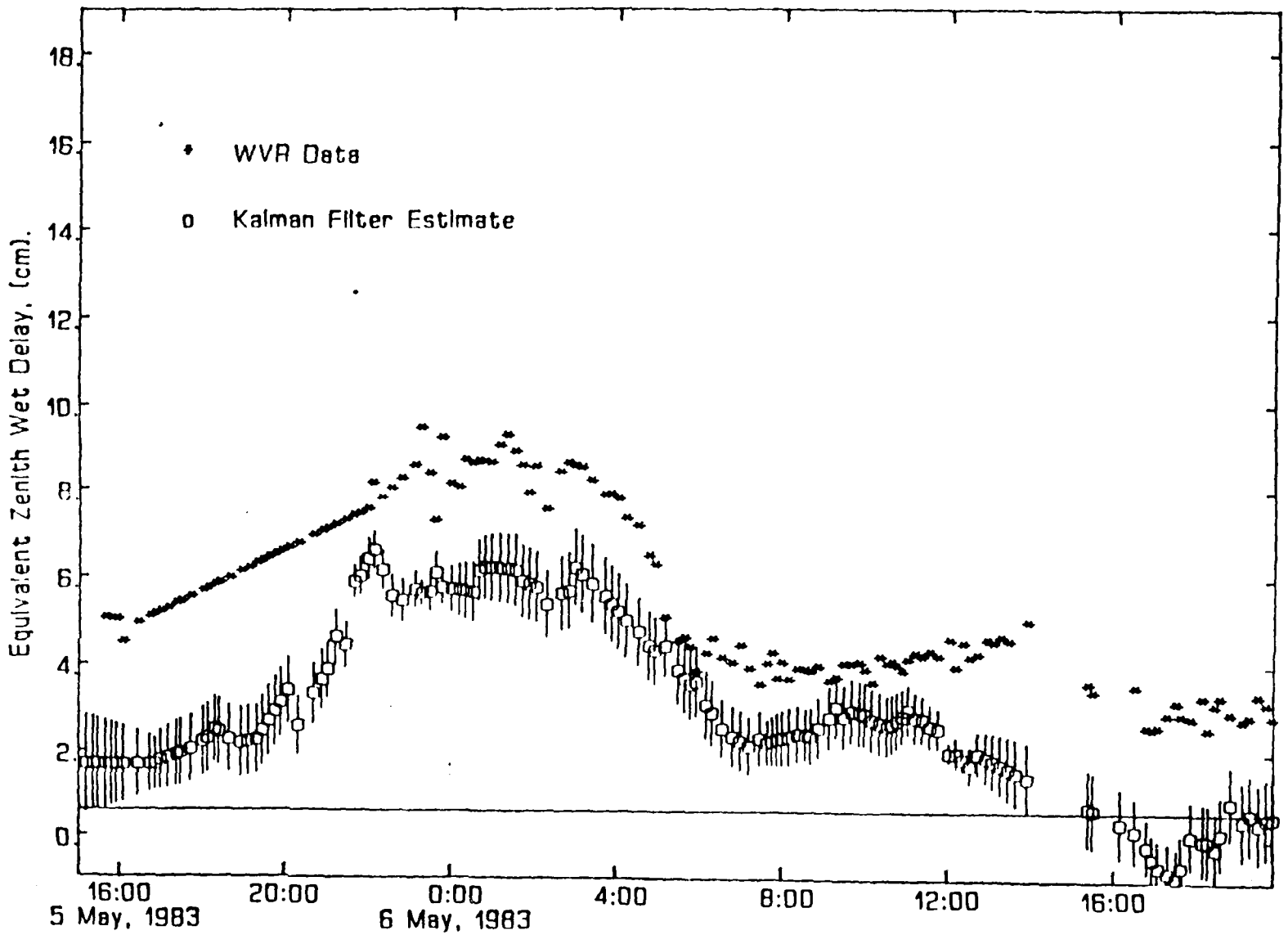
WVR Data
Kalman Filter Estimate
Equivalent Zenith Wet Delay, (cm).
18
16
14
12
10
8
6
4
2
0
16:00
5 May, 1983
20:00
0:00
6 May, 1983
4:00
8:00
12:00
16:00

FIGURE 2

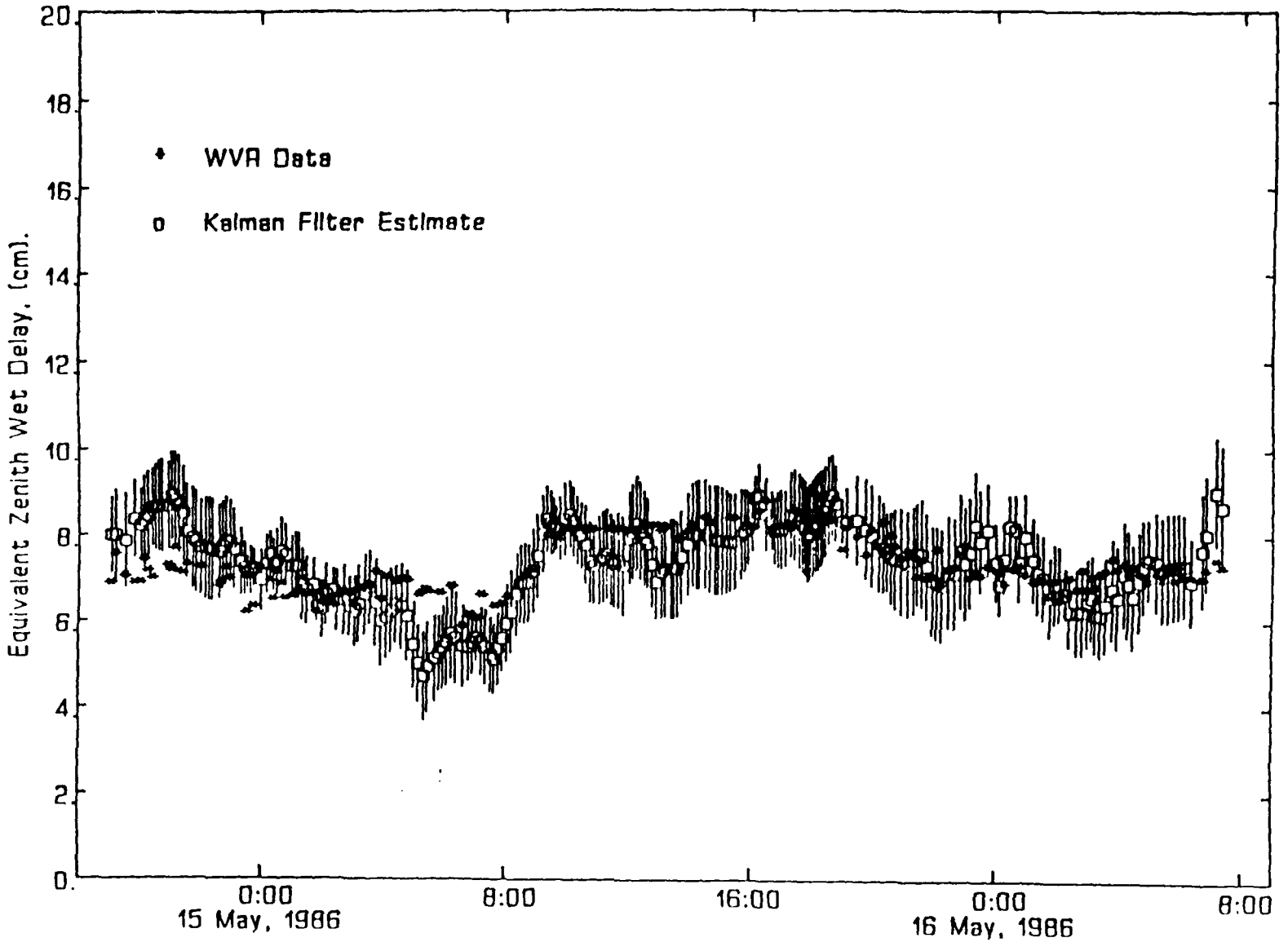
20
18
16
14
12
10
8
6
4
2
0
WVR Data
Kalman Filter Estimate
Equivalent Zenith Wet Delay, (cm).
0:00
15 May, 1986
8:00
16:00
0:00
16 May, 1986
8:00

FIGURE 3

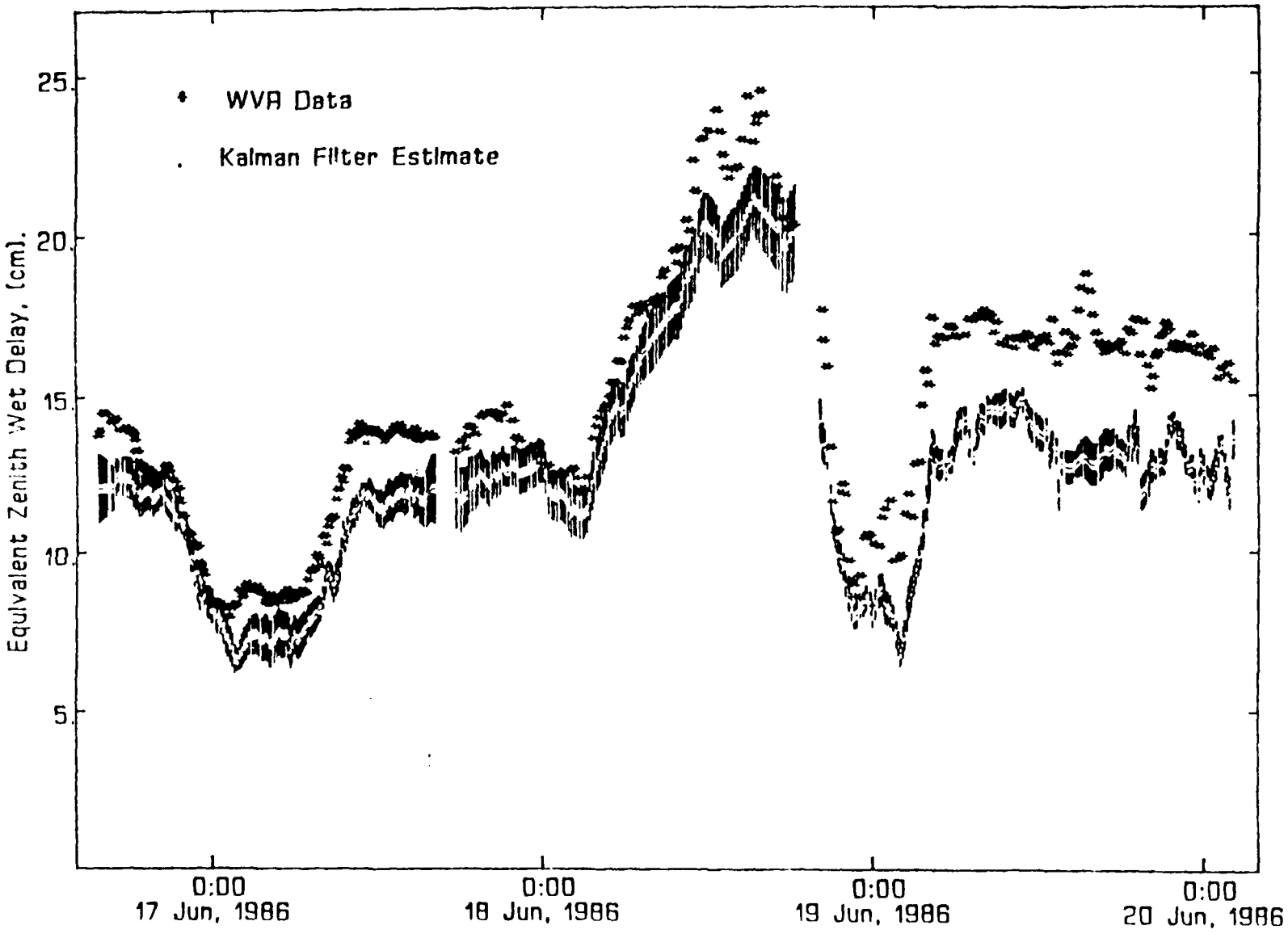
WVR Data
Kalman Filter Estimate
Equivalent Zenith Wet Delay, (cm).
25.
20.
15.
10.
5.
0:00
17 Jun, 1986
0:00
18 Jun, 1986
0:00
19 Jun, 1986
0:00
20 Jun, 1986

FIGURE 4

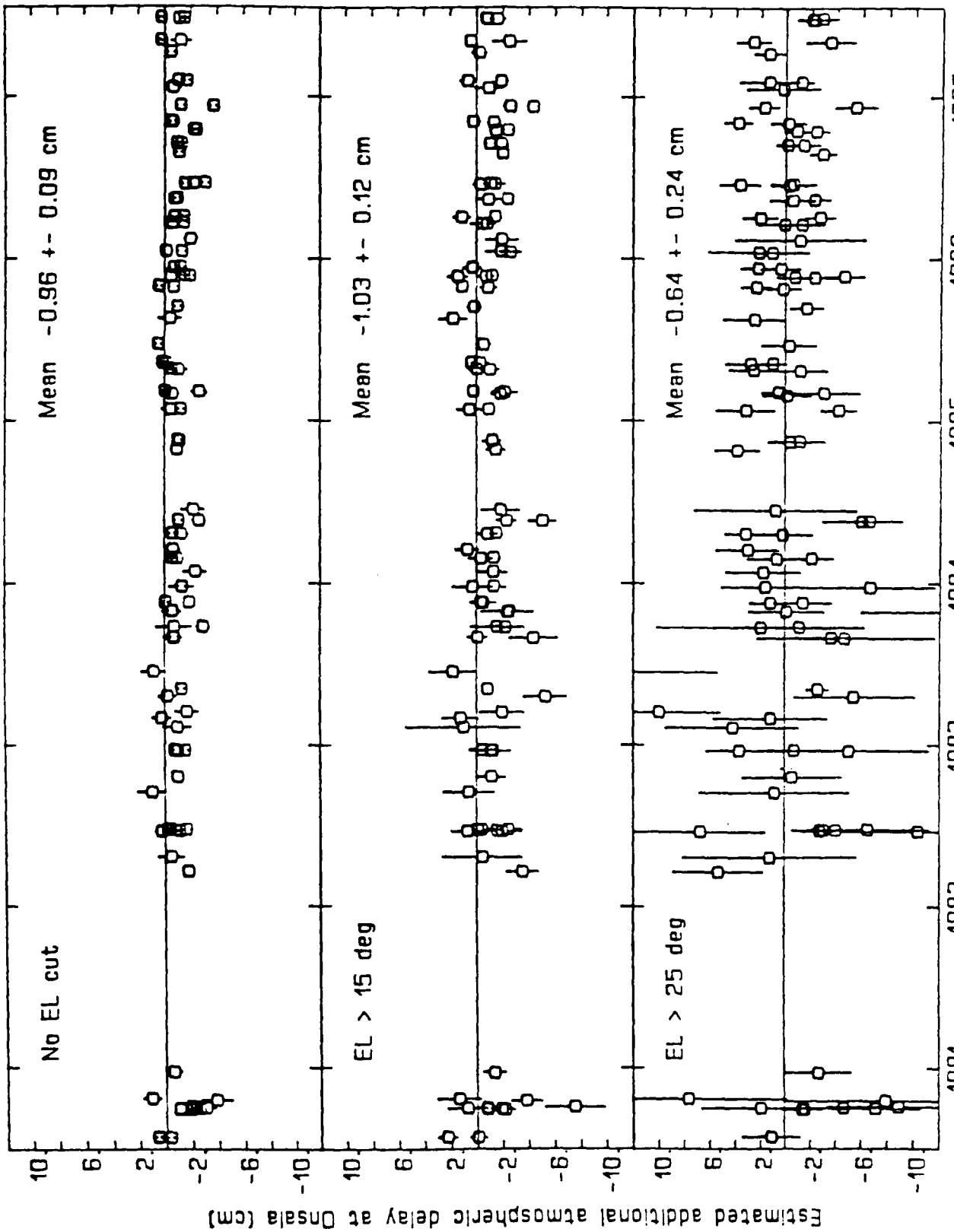
No EL cut
Mean -0.96 +- 0.09 cm
EL > 15 deg
Mean -1.03 +- 0.12 cm
EL > 25 deg
Mean -0.64 +- 0.24 cm
10
6
2
-2
-6
-10
1981
1982
1983
1984
1985
1986
1987
Estimated additional atmospheric delay at Onsala (cm)

FIGURE 5

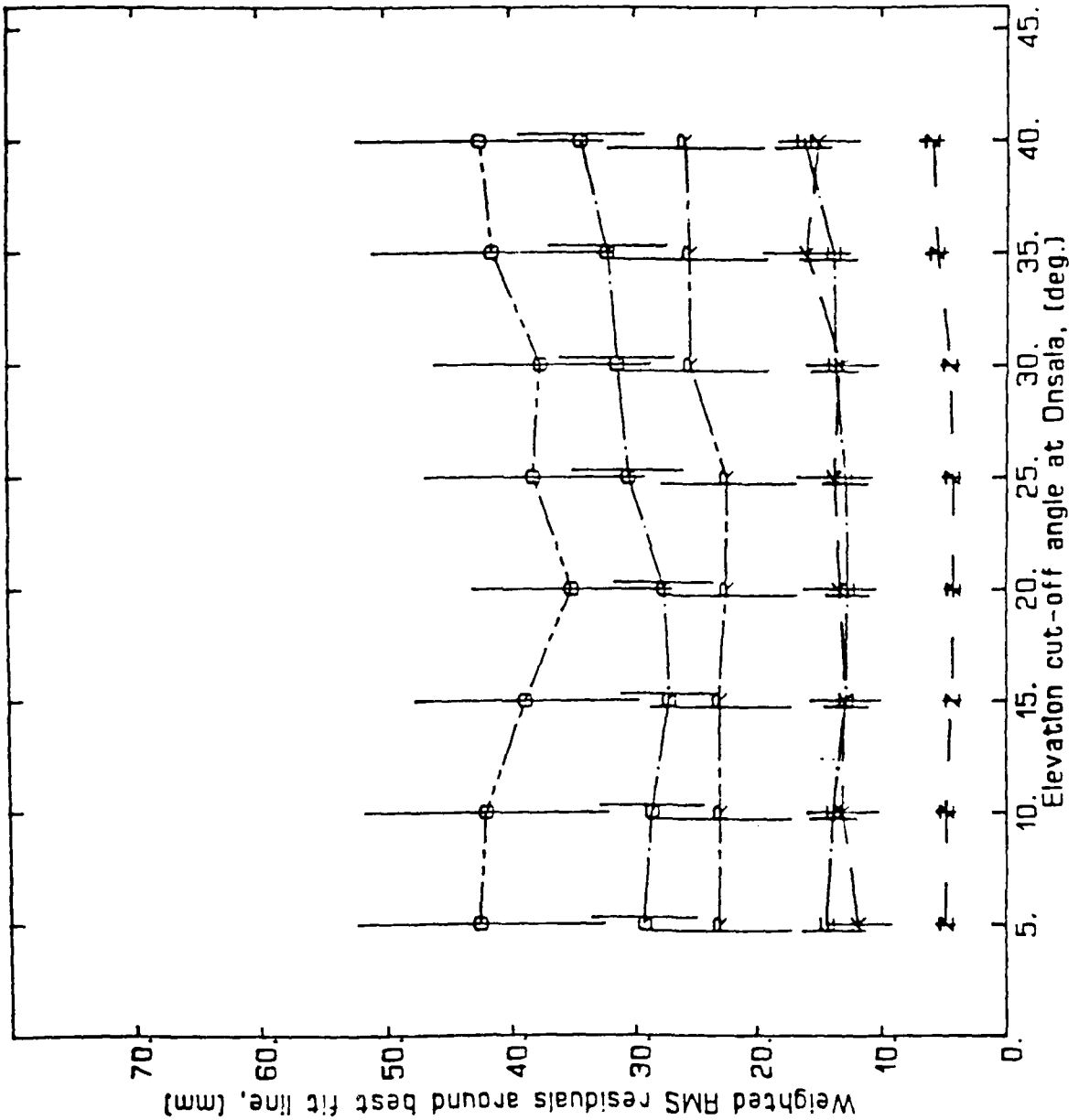
Weighted RMS residuals around best fit line, (mm)
0.
10.
20.
30.
40.
50.
60.
70.
5.
10.
15.
20.
25.
30.
35.
40.
45.
Elevation cut-off angle at Onsala, (deg.)

FIGURE 6

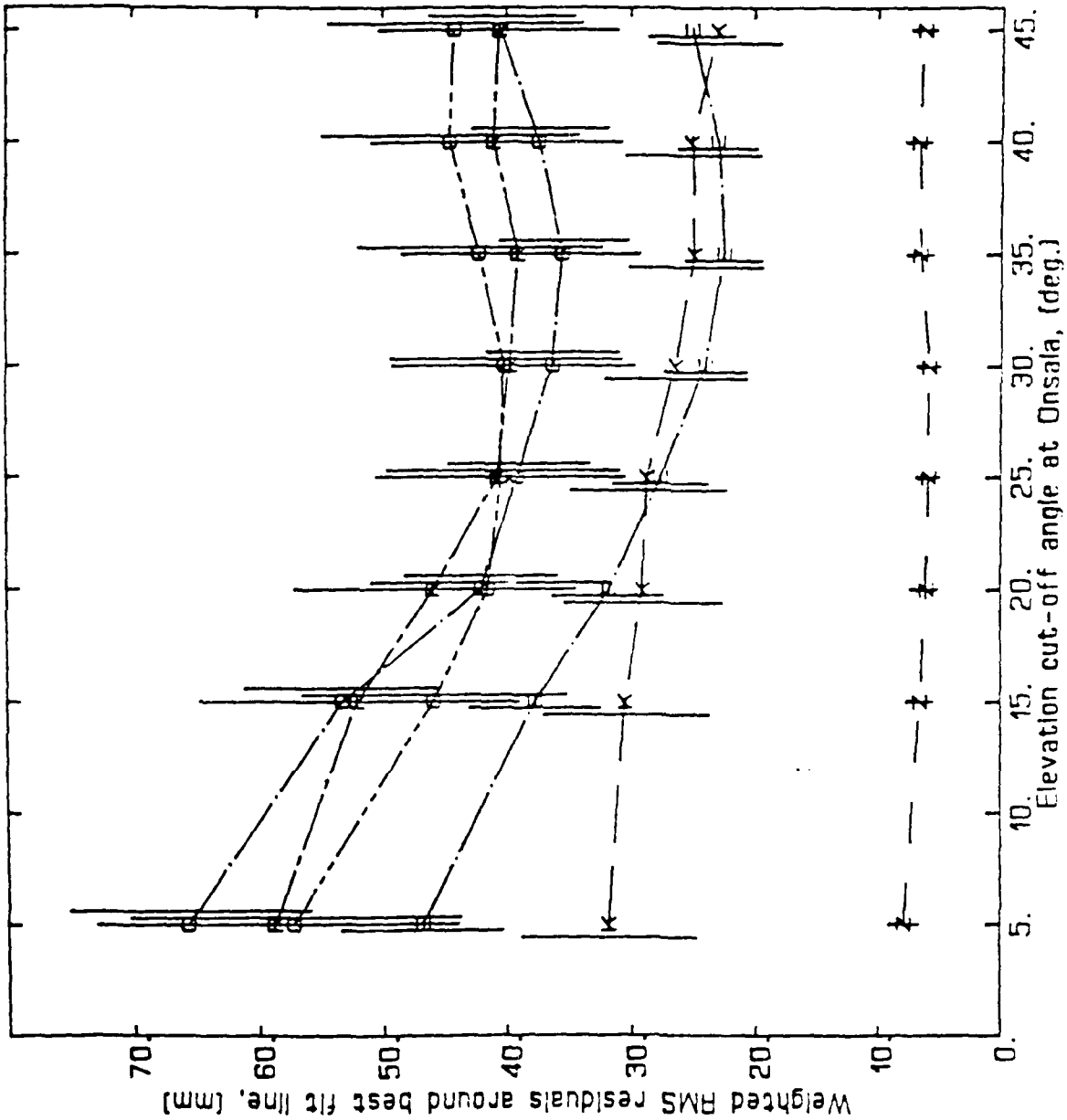
Weighted RMS residuals around best fit line, [mm]
0.
10.
20.
30.
40.
50.
60.
70.
5.
10.
15.
20.
25.
30.
35.
40.
45.
Elevation cut-off angle at Onsala, (deg.)

FIGURE 7

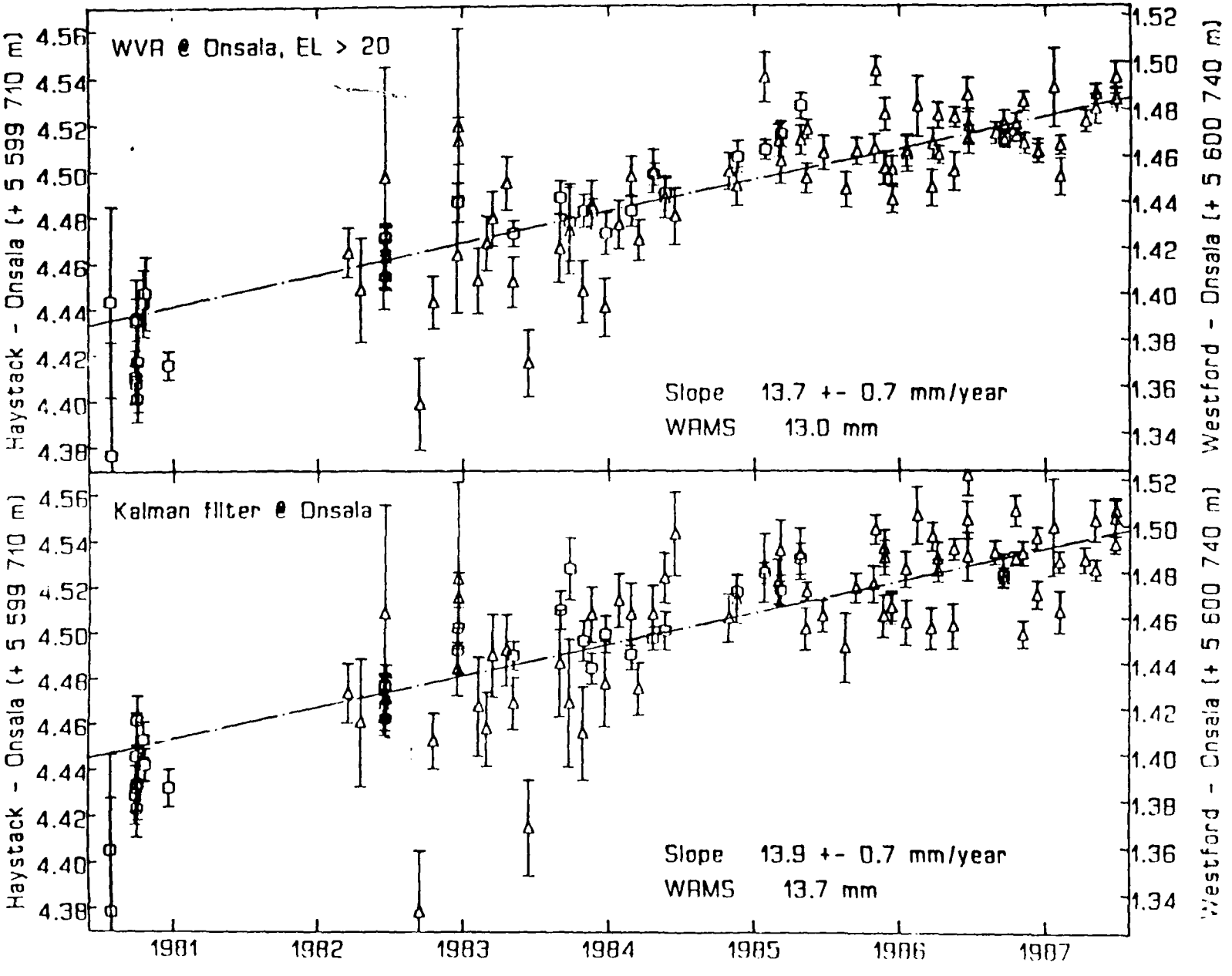
WVR @ Onsala, EL > 20
Slope 13.7 +- 0.7 mm/year
WRMS 13.0 mm
Kalman filter @ Onsala
Slope 13.9 +- 0.7 mm/year
WRMS 13.7 mm
Haystack - Onsala (+ 5 599 710 m)
Westford - Onsala (+ 5 600 740 m)
4.56
4.54
4.52
4.50
4.48
4.46
4.44
4.42
4.40
4.38
1.52
1.50
1.48
1.46
1.44
1.42
1.40
1.38
1.36
1.34
1981
1982
1983
1984
1985
1986
1987

FIGURE 8

VLBI geodesy: 2 parts-per-billion precision in length determinations for transcontinental baselines

J.L. Davis, T.A. Herring, and I.I. Shapiro
Harvard-Smithsonian Center for Astrophysics
Cambridge, Massachusetts 02138

ABSTRACT. We have used very-long-baseline interferometry (VLBI) to make twenty-two independent measurements, between September 1984 and December 1986, of the length of the 3900-km baseline between the Mojave site in California and the Haystack/Westford site in Massachusetts. These experiments differ from the typical geodetic VLBI experiments in that a large fraction of observations are obtained at elevation angles between 4° and 10°. Data from these low elevation angles allows the vertical coordinate of site position, and hence the baseline length, to be estimated with greater precision. For the sixteen experiments processed thus far, the weighted root-mean-square scatter of the estimates of the baseline length is 8 mm. We discuss these experiments, the processing of the data, and the resulting baseline length estimates.

1. INTRODUCTION

In recent years, the precision of estimates of baseline length obtained from the analysis of Mk-III very-long-baseline interferometry (VLBI) data has passed below the level of 10 parts-per-billion. The limiting source of error continues to be the atmosphere. The effects of atmospheric errors on estimates of baseline length are discussed in Lanyi [1984], Davis *et al.* [1985], Davis [1986], Herring [1986], and Treuhaft and Lanyi [1987]. The typical treatment of atmospheric propagation delay in the analysis of geodetic VLBI data involves the use of surface meteorological measurements (and possibly radiometric measurements; see Elgered *et al.* [1987]) to determine an *a priori* value for the zenith propagation delay, and the use of a mapping function. (The mapping function describes the elevation-angle dependence of the propagation delay, *i.e.*, the number of air masses traversed.) Corrections to the *a priori* value of the zenith delay are then estimated, along with the relevant geodetic parameters, from the VLBI data.

The unique elevation-angle dependence of the atmospheric propagation delay allows a precise estimate to be made of the zenith-delay corrections. However, the sensitivity of the VLBI group-delay measurement to a change in the zenith delay is highly correlated with the sensitivity of the group delay to a change in the vertical coordinate of site position for small ranges of air mass. By observing sources at low elevation angles, we can decrease the correlation of the estimates of the zenith-delay corrections with those of the vertical coordinate of site positions, and thereby obtain a more precise estimate of those (and other) parameters. Nevertheless, many schedules for geodetic VLBI experiments include no observations below about 10° elevation at any site. This omission is primarily intended to *avoid* the effects of errors in the mapping function used, since such errors are generally worse at lower elevations. (It is harder to predict atmospheric properties at greater horizontal distances from the site.) We therefore pose the question: What is the "optimum" minimum elevation angle to minimize errors in baseline-length estimates?

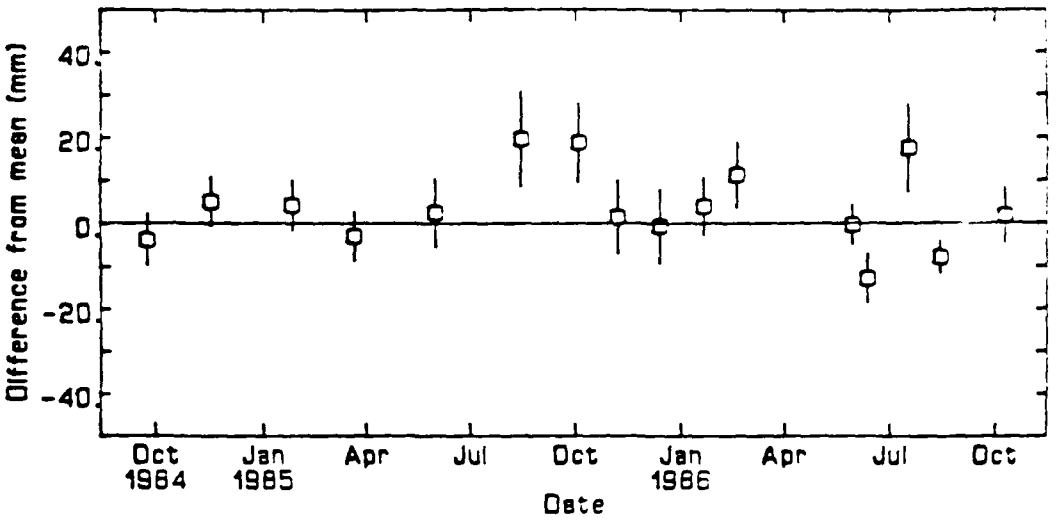

Figure 1. Estimates of the length of the baseline from Haystack/Westford to Mojave (see text). A mean value of 3,904,144,248 mm has been subtracted from the values shown.

2. DESCRIPTION OF EXPERIMENTS and RESULTS

In order to study this question, we designed VLBI experiments known as "low-elevation" experiments in reference to their scheduling strategy: the attempt is made to observe low in the sky as frequently as possible, within the limits of the antennas used. For the standard set of low-elevation experiments, we used the Mojave site ($\epsilon_{min} = 8°$) in California and the Haystack/Westford site ($\epsilon_{min} = 4°$) in Massachusetts.

The processing of the data from these experiments differed in several respects from the processing which we employed several years ago (see, *e.g.*, Clark *et al.* [1985]) for geodetic VLBI data. A new mapping function for the dry atmosphere, developed by Davis *et al.* [1985], and accurate to about 10 mm at 5° elevation for a wide range of atmospheric conditions, was used. Another improvement was the use of a Kalman filter to estimate clock offsets and zenith delay corrections. Each of these corrections is modeled as a time-varying stochastic process, the statistics of which are deduced from other sources; the values of the corrections for the epochs of the VLBI observations are estimated by the Kalman filter. Finally, we used radiometric data to estimate the "wet delay" when these data are available.

In Figure 1, we present the estimates of the Haystack-Mojave baseline lengths as a function of experiment date. The error bars represent the standard deviation of the estimate of the baseline length, deduced from the propagation of the stochastic errors involved. These errors include the the measurement errors of the group-delay observations and the stochastic behavior of the clocks and atmospheres. The weighted root-mean-square scatter of the estimates about their weighted mean is 8 mm, representing a fractional repeatability of 2 parts-per-billion.

This work was supported by Air Force Geophysics Laboratory contract F-19628-86-K-0025; NASA grant NAG5-538; and NSF grants EAR-83-06380 and EAR-86-18989.

Clark, T.A. *et al.*, *IEEE Trans. GARS* GE-23, 438–449, 1985.
Davis, J.L., T.A. Herring, I.I. Shapiro, A.E.E. Rogers, G. Elgered, *Radio Science* 20, 1593–1607, 1985.
Davis, J.L., U.S. Air Force report AFGL-TR-86-0243, 1986. ADA178405
Elgered, G., J.L. Davis, T.A. Herring, I.I. Shapiro, this volume, 1987.
Herring, T.A., *J. Geophys. Res* 91, 9177–9182, 1986.
Lanyi, G.E., *Proc. Int. Symp. Space Tech. Geodyn.*, IAG/COSPAR,2, 184–195, 1984.
Treuhaft, R.N., G.E. Lanyi, *Radio Science* 22, 251–265, 1987.

VLBI studies of the nutations of the earth

T. A. Herring, Harvard-Smithsonian Center for Astrophysics
60 Garden Street
Cambridge, MA. 02138

ABSTRACT. The application of very-long-baseline interferometry (VLBI) to the study of the nutations of the earth has yielded unprecedented accuracy for the experimental determination of the coefficients of the nutation series. The analysis of six years of VLBI data has yielded corrections to the coefficients of the seven largest terms in the IAU 1980 nutation series with periods of one year or less, with accuracies approaching the truncation error of this nutation series (0.1 mas). The nutation series coefficients computed from the VLBI data, and those obtained from theoretical considerations (the IAU 1980 nutation series), are in excellent agreement. The largest corrections are to the coefficients of the retrograde annual nutation [2.0 ± 0.1 mas], the prograde semiannual nutation [(0.5 - i 0.4) ± 0.1 mas], and the prograde 13.7 day nutation [-0.4 ± 0.1 mas]. (The imaginary term for the semiannual nutation represents a term 90° out-of-phase with the arguments of the nutation series.) The geophysical implications of these results are currently under active investigation. We discuss the methods used to extract the nutation information from the VLBI data, the calculations of the uncertainties of the resultant corrections to the coefficients of the nutation series, and the current research into the nutations of the earth.

1. INTRODUCTION

The determination of the coefficients of the nutation series using very-long-baseline interferometry data has been discussed recently in a number of papers (*Herring et al.*, 1983; *Gwinn et al.*, 1984; *Herring et al.*, 1985; *Eubanks et al.*, 1985; *Gwinn et al.*, 1986; *Herring et al.*, 1986a; *Herring et al.*, 1986b; and *Himwich et al.*, 1986). A detailed description of the analysis techniques used for determining the corrections to the coefficients of the nutation series is given in *Herring et al.*, 1986a. The interpretation of the results given in *Herring et al.*, 1986a is discussed in detail by *Gwinn et al.*, 1986. The interpretation of these results has also been discussed by *Wahr and Bergen et al.*, 1986; *Yoder and Ivinus*, 1986; and *Yoder and Ivinus*, 1987. Here we review briefly the procedures used to estimate the corrections to the coefficients of the nutations, and we present the results obtained from the analysis of 412 VLBI experiments obtained during the 6.5 year period between July 1980 and February 1987.

M. J. Reid and J. M. Moran (eds.), The Impact of VLBI on Astrophysics and Geophysics, 371–375

2. DATA ANALYSIS TECHNIQUE

The techniques we have used to estimate corrections to the IAU 1980 nutation series have been discussed in *Herring et al.*(1985) and *Herring et al.*(1986a). For each VLBI observing session (typically of 24 hours duration), we estimate corrections, $\delta\Delta\psi$ and $\delta\Delta\epsilon$, to the nutation angles computed from the IAU 1980 nutation series. In a post-processing operation, we use these nutation-angle corrections to estimate corrections to the coefficients of certain terms in the nutation series. An alternative technique is to directly estimate the corrections to coefficients of the nutation series from the VLBI data themselves. Results obtained using this technique have been presented by *Himwich et al.*, 1986.

The nutation-angle corrections are not only used to estimate the corrections to the coefficients of the nutation series, but they are also be used to study the noise characteristics of the nutation estimates (see *Herring et al.*,1986a), and to study phenomena not explicitly included in the standard nutation series such as the "free core-nutation" (see *Herring et al.*, 1986b). In particular, we will discuss the power-spectral density (PSD) function of the nutation-angle corrections. The calculation of the PSD function from the nutation-angle corrections have been discussed in *Herring et al.*, 1985. The technique we adopt is to "lightly" smooth the nutation-angle corrections using a Gaussian filter with a full-width-at-half-maximum (FWHM) of 5 days, and to then compute the PSD function from these uniformly spaced smoothed values (5 day spacing). The (assumed uncorrelated) noise in the nutation-angle corrections is propagated through the smoothing and the fast fourier transform (FFT) algorithms to compute the 99.5% confidence limit for the PSD function.

3. RESULTS

The VLBI data we have analyzed are from 412 observing sessions carried out by the NASA Crustal Dynamics Project and the NGS IRIS program between July 1980 and February 1987. This data set is an extension of those discussed in *Herring et al.*(1985) and *Herring et al.*(1986a and b). In Table 1, we give the estimates of the amplitudes of the circular nutations that can be resolved with the limited temporal range of the VLBI data. The values for $\delta\Delta\epsilon$ and $\delta\Delta\psi\sin\epsilon_0$ we used to obtain these amplitude estimates are shown in Figure 1. The PSD function computed from the nutation-angle corrections shown in Figure 1 is shown in Figure 2. The three largest peaks in the PSD function correspond to the three largest corrections to the coefficients of the nutation series given in Table 1. There is also a large peak corresponding to the retrograde frequency closest to 1 cycle per sidereal day. Any corrections to the long period nutations (18.6 and 9.3 years) would all appear in this term. With only 6.5 years of data we can not yet reliably estimate corrections to the nutation series terms with these long periods. The remainder of the PSD function appears to be consistent with the white-noise statistics used to compute the 99.5% confidence interval.

The results given in Table 1 are very consistent with previously published results within the uncertainties of these earlier analyses. The correction to the retrograde annual nutation has been interpreted as being due to the effects of the earth's fluid core being more strongly coupled to the mantle than was inferred for the calculation of the IAU 1980 nutation series (*Gwinn et al.*, 1986). The corrections to the prograde semiannual term are partly due the coupling of the fluid core to the mantle and partly due to the effects of ocean tides on the nutations (*Sasao and Wahr*, 1981). The correction to the 13.7 day prograde term has not

TABLE 1. Estimates of Corrections to Amplitudes of Circular Nutations of IAU 1980 Nutation Series (*Wahr*, 1981).

Period in inertial space, days	Observed Amplitude, mas	Corrections* In-Phase δa_r, mas	Corrections* Out-of-Phase δa_i, mas
182.6 prograde	-548.62	0.45	-0.41
182.6 retrograde	-24.63	-0.11	-0.07
13.7 prograde	-94.45	-0.37	-0.00
13.7 retrograde	-3.63	-0.03	0.05
365.3 prograde	25.71	0.05	0.15
365.3 retrograde	-33.13	-2.07	0.36
27.6 prograde	14.50	-0.02	0.00
27.6 retrograde	-13.79	0.03	-0.01
121.7 prograde	-21.56	-0.08	-0.03
121.7 retrograde	-0.95	-0.04	-0.03
9.1 prograde	-12.53	-0.10	0.00
9.1 retrograde	-0.43	-0.01	-0.02
31.8 prograde	3.19	-0.01	-0.02
31.8 retrograde	-3.02	0.07	0.00
433.2 prograde	0.06†	-0.06	-0.00
433.2 retrograde FCN	0.33†	0.32	-0.04

*The standard deviation of each correction is estimated to be 0.10 mas. The standard deviations are obtained using the techniques described in *Herring et al.* (1986), with the root-sum-squares addition of a contribution of 0.07 mas to account for (i) the effects of the truncation of the IAU 1980 nutation series to the nearest 0.1 mas, (ii) the possible effects of atmospheric excitation of the nutations, and (iii) the effects of ocean and earth tide modeling errors in the analysis of the VLBI data. See also *Herring et al.* (1986) for definitions of the quantities listed.

†The amplitudes of these terms are the root-sum-squares of the amplitudes of the real and imaginary components.

been satisfactorily explained. Since this nutation term is the one most affected by the elasticity of the earth, the correction may arise from the treatment of elasticity or the neglect of the effects of anelasticity in the IAU nutation series. The root-mean-square scatter of the remaining 25 corrections given in Table 1 is 0.06 mas, which is consistent with our estimated uncertainties of 0.10 mas.

4. CONCLUSION

The quality of the VLBI estimates of the corrections to the nutation series will improve as further VLBI experiments are carried out. The VLBI data from the international earth rotation service will continue to provide high quality measurements of the nutation angles on a regular basis (once every 5 days). These data and those obtained by the NASA Crustal Dynamics Project will ensure that the coefficients of selected terms in the nutation series will be determined with precisions of less than 0.1 mas. However, the current nutation series is truncated at 0.1 mas, and thus, will soon be the limiting error source in the interpretation of the corrections to the nutation series. Since all modern nutation series are obtained by convolving the response function of a "realistic" model earth with the nutations of a rigid earth, we will soon start developing a rigid-earth nutation

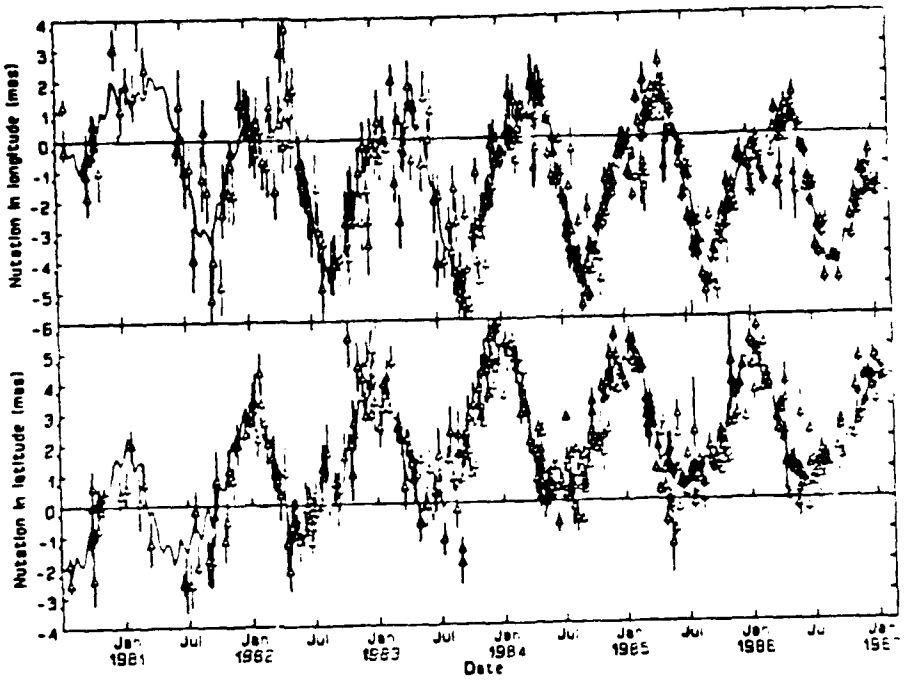

Figure 1. Estimates of $\delta\Delta\epsilon$ and $\delta\Delta\psi\sin\epsilon_o$ from the VLBI data analyzed in this paper. The solid line in each figure is computed from the corrections given in Table 1 and from long-period terms (periods $\geq$ 18.6 years) which are not given in the table because their values are highly correlated and the estimates are not considered reliable.

---

series with an accuracy of 0.01 mas. This new nutation series will provide an accurate framework in which the observed nutations of the earth can be compared with that computed from geophysical theory.

5. ACKNOWLEDGMENTS

This work was supported by the Air Force Geophysics Laboratory, contract F-19628-86-K-0025; NASA grant NAG5-538; and NSF grants EAR-83-06359 and EAR-86-18989.

6. REFERENCES

Eubanks, T.M. *et al.*, in "Proc. of the international conference on earth rotation and the terrestrial reference frame", Ohio State University, 326-340, 1985.
Gwinn, C.R. *et al.*, *EOS*, **65**, 859, 1984.
Gwinn, C.R. *et al.*, *J. Geophys. Res.*, **91**, 4755-4765, 1986.
Herring, T.A. *et al.*, *EOS*, **64**, 674, 1983.
Herring, T.A. *et al.*, in "Proc. of the international conference on earth rotation and the terrestrial reference frame", Ohio State University, 307-325, 1985.

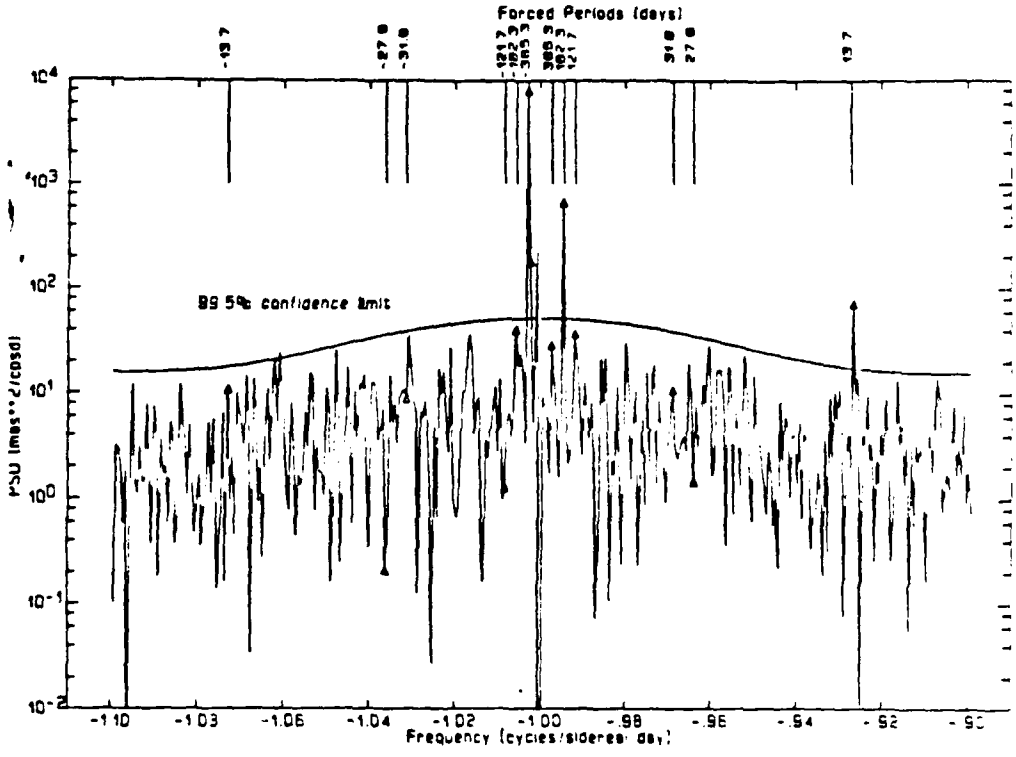

Figure 2. The power-spectral-density (PSD) function of the nutation-angle corrections shown in Figure 1. The decrease in power in the PSD function and in the 99.5% confidence limit with increasing frequency away from -1 cycle per sidereal day (cpsd) is due to use of a (5 day FWHM) Gaussian filter. The frequency spacing in the PSD function is 1/1830 cpsd. At the top of the figure we have shown the frequency positions of some of the major terms in the nutation series. We have also marked the frequency components in the PSD function closest to these frequencies with triangles.

Herring, T.A. *et al.*, *J. Geophys. Res.*, **91**, 4745–4754, 1986a.
Herring, T.A. *et al.*, in "Proc. of IAU Symp. No. 128", 1986b.
Himwich, W.E. *et al.*, in "Proc. of IAU Symp. No. 128", 1986.
Sasao, T. and J.M.Wahr, *Geophys. J. Roy. Astr. Soc.*, **64**, 729–746, 1981.
Wahr, J.M. and T.Sasao, *Geophys. J. Roy. Astr. Soc.*, **64**, 747–765, 1981.
Wahr, J.M. and Z. Bergen, *Geophys. J. R. Astr. Soc.*, **87**, 633-668, 1986.
Yoder, C.F. and E.R. Ivinis, in "Proc. of IAU Symp. No. 128", 1986.
Yoder, C.F. and E.R. Ivinis, in "Proc. of IAU Symp. No. 129", 1987.

BOUND ON THE AMPLITUDE OF THE EARTH'S FREE CORE-NUTATION

T. A. Herring, C. R. Gwinn, B.A. Buffett, and I. I. Shapiro
Harvard-Smithsonian Center for Astrophysics
60 Garden Street
Cambridge, MA. 02138

ABSTRACT. We analyzed six years of very-long-baseline interferometry (VLBI) data and determined corrections to the coefficients of the seven terms with the largest amplitudes in the IAU 1980 nutation series. Our analysis yields results consistent with earlier analyses of smaller sets of VLBI data, within the uncertainties of the latter. Here, we restrict discussion to the freely excited core–nutation or "free core–nutation" (FCN). Our analysis yields an estimate of 0.33 ± 0.12 mas for an assumed constant amplitude of the FCN, which allows us to place an upper bound on it of 0.6 mas (99.5% confidence limit). We also studied possible temporal variations of the complex amplitude of the FCN by modeling it as a stochastic process with a white noise excitation. We detected no statistically significant variations of this amplitude for the six-year interval spanned by the VLBI data. However, in the neighborhood of one cycle per day, the power spectral density of the atmospheric surface loading is estimated from global weather data to be 0.24 $(\text{g cm}^{-2})^2$ day, about five times larger than the largest such power spectral density that would be consistent with the upper bound on the amplitude of the FCN placed by the VLBI data. Thus, we conclude that this estimate is too high and that, if the FCN were excited by surface loads with frequencies near one cycle per day, then the power spectral density of these loads must be <0.06 $(\text{g cm}^{-2})^2$ day (99.9% confidence limit).

1. INTRODUCTION

The recent investigations of the nutations of the earth using VLBI data (*Herring et al.*, 1983; *Gwinn et al.*, 1984; *Herring et al.*, 1985; *Eubanks et al.*, 1985; and *Herring et al.*, 1986) have all disclosed corrections to the coefficients of the terms in the IAU 1980 nutation series corresponding to the retrograde annual nutation and the prograde semiannual nutation. These corrections can be partially explained by changing the resonance frequency (in a frame rotating with the earth) of the "core nutation" from $-(1+\frac{1}{460})$ cycles per sidereal day (cpsd) to $-(1+\frac{1}{433})$ cpsd (*Gwinn et al.*,1986). Other phenomena contributing significantly to the corrections might be ocean tides (*Wahr and Sasao*, 1981) and the anelasticity of the earth's mantle (*Wahr and Bergen, private communication*, 1986). These latter two effects are not, however, nearly large enough by themselves to explain the ≈ 2 mas correction to the amplitude of the retrograde annual nutation. These small corrections aside, the overall agreement between the VLBI results and the IAU 1980 nutation series is evidence for the existence of the predicted effect of the core–nutation resonance on the earth's rotation: this resonance contributes as much as 17 mas to

A. K. Babcock and G. A. Wilkins (eds.), The Earth's Rotation and Reference Frames for Geodesy and Geodynamics, 293–299.

the nutation series, in particular to the semiannual term. Nonetheless, the free excitation of this mode has never been unambiguously detected. Prior analyses of VLBI data have placed only upper bounds of under 1 mas on the amplitude of this free core nutation (FCN) [*Herring et al.*, 1985; *Eubanks et al.*, 1985; and *Herring et al.*, 1986].

In this paper, we examine the FCN in more detail. In particular, we investigate the possibility that our single ("average") estimate of the amplitude of the FCN may be significantly less than the maximum value reached by this amplitude during the six-year interval spanned by the VLBI data, due to large fluctuations in this (complex) amplitude during this interval. This situation could arise if the FCN were heavily damped and highly excited. An estimated lower bound on the damping time, combined with an independent estimate of the expected amplitude of the FCN can be used to quantify statistically the possible fluctuations in this amplitude. We can obtain a lower bound for the damping time from the VLBI estimate of the amplitude of the out-of-phase component of the retrograde annual nutation. An estimate of the expected amplitude of the excitation of the FCN can be obtained from other geophysical data. In particular, we take the expected amplitude of the FCN from the magnitude obtained by *Eubanks et al.*(1985) of the power spectral density, at nearly diurnal periods, of the P_{21} component of the atmospheric pressure loading of the earth's surface (see *Wahr and Sasao* (1981) for normalization of spherical harmonics).

2. DATA ANALYSIS TECHNIQUE

The techniques we have used to estimate corrections to the IAU 1980 nutation series have been discussed in *Herring et al.*(1985) and *Herring et al.*(1986). For each VLBI observing session (typically of 24 hours duration), we estimate corrections, $\delta\Delta\psi$ and $\delta\Delta\epsilon$, to the nutation angles computed from the IAU 1980 nutation series. In a post-processing operation, we use these nutation-angle corrections to estimate corrections to the coefficients of certain terms in the nutation series. The analysis used in this paper is similar to our previous analyses except that here we allow our model of the complex amplitude of the FCN to vary stochastically during the interval spanned by the data set. A Kalman filter (see, *e.g.*, *Liebelt*, 1967) was used to estimate simultaneously the time-dependent complex amplitude of the FCN, and the corrections to the coefficients of selected terms in the IAU 1980 nutation series.

The stochastic model used to represent the complex amplitude of the FCN was

$$\tilde{\zeta}(t+\Delta t) = \tilde{\zeta}(t)e^{-\alpha\Delta t} + \delta\tilde{\zeta}(t) \cdots \quad (1)$$

where, respectively, $\tilde{\zeta}(t)$ and $\tilde{\zeta}(t+\Delta t)$ are the complex values of the FCN at times t and $t+\Delta t$; α (>0) is the inverse damping time for the FCN and stems from the imaginary, or dissipative, part of the FCN resonance frequency; and $\delta\tilde{\zeta}(t)$ is the complex excitation, integrated over the interval t to $t+\Delta t$ $(\Delta t \ll \alpha^{-1})$. The corresponding contributions of the FCN to the nutation angles are

$$\delta\Delta\epsilon_{FCN}(t) = -\zeta_r(t)\cos\big((\Omega+\omega_{FCN})t\big) - \zeta_i(t)\sin\big((\Omega+\omega_{FCN})t\big) \quad (2)$$

and

$$\delta\Delta\psi_{FCN}(t)\sin\epsilon_o = -\zeta_r(t)\sin\big((\Omega+\omega_{FCN})t\big) + \zeta_i(t)\cos\big((\Omega+\omega_{FCN})t\big), \quad (3)$$

where, respectively, $\zeta_r(t)$ and $\zeta_i(t)$ are the real and imaginary parts of $\tilde{\zeta}(t) = \zeta_r(t) - i\zeta_i(t)$; t is sidereal time (measured for convenience from the epoch J2000); Ω

is the earth's rotation rate; and ω_{FCN} is the real component of the FCN frequency. To apply a Kalman filter to the estimates of $\delta\Delta\epsilon(t)$ and $\delta\Delta\psi(t)$ obtained from the VLBI data, we need to establish the statistical properties of the excitation of the FCN. However, we do not know the excitation mechanism for the FCN. The most efficient mechanism seems to be through surface loading (*Sasao and Wahr*, 1981). But, very little is known about the properties of non-tidal surface loading with periods near one day. Likely candidates for the excitation are loads from atmospheric pressure variations, and, possibly, from sea level changes (*Sasao and Wahr*, 1981). Since we know so little about the spectra of these excitations, we will make the simple assumption that all of them have white-noise spectra for periods near one day. We will characterize the amplitude of the white-noise excitation by its variance, $\sigma_\zeta^2 = \langle \delta\tilde{\zeta}(t)\delta\tilde{\zeta}^*(t)\rangle$, where * denotes complex conjugation, and $\langle\rangle$ denotes expectation.

The magnitude of σ_ζ^2 can be established by balancing the power input into the FCN by the excitation with that dissipated. From equation (1), we have for steady-state conditions (assuming $\alpha\Delta t \ll 1$):

$$\sigma_\zeta^2 = 2\langle\tilde{\zeta}\tilde{\zeta}^*\rangle\alpha\Delta t. \tag{4}$$

Therefore, if we know α and the expectation of the square of the magnitude of the (integrated) complex excitation of the FCN, we can compute the variance of the white-noise excitation to be used in the Kalman filter.

3. RESULTS

The VLBI data we have analyzed are from 370 observing sessions carried out by the NASA Crustal Dynamics Project and the NGS IRIS program between July 1980 and August 1986. This data set is an extension of those discussed in *Herring et al.*(1985) and *Herring et al.*(1986). In Table 1, we give the estimates of the amplitudes of the circular nutations that can be resolved with the limited temporal range of the VLBI data. The values for $\delta\Delta\epsilon$ and $\delta\Delta\psi\sin\epsilon_o$ we used to obtain these amplitude estimates are shown in Figure 1. These amplitude results are based on the assumption that the amplitude of the FCN was constant for the six years spanned by the data set, i.e. that σ_ζ^2=0, whence the Kalman filter solution reduces to conventional weighted-least squares. In this solution, we not only estimated the amplitude of the FCN, but also the amplitude of a prograde ("control") term with the frequency $-(1-\frac{1}{433})$ cpsd. Since no resonance is thought to exist for any such prograde term, any signal at this frequency is probably due to noise or to model deficiencies, and could be used as a measure of the uncertainty affecting the estimate of the FCN amplitude. The resultant estimates of the amplitudes of the FCN and the prograde terms are, respectively, 0.33 ± 0.12 and 0.04 ± 0.12 mas.

The amplitude of the FCN can also be estimated from other data. *Eubanks et al.* (1985) have estimated from global weather data that the power spectral-density (PSD) of the P_{21} component of the atmospheric pressure field is 0.24 (gm cm^{-2})^2 day. (No uncertainty for this value is given by the authors. However, the estimate is stated to be "conservative.") This PSD, combined with the lower bound for damping time deduced from the VLBI data (see below), suggests that the FCN amplitude should be $\geq$0.8 mas (see *Sasao and Wahr*, 1981 for computation methods). From this lower bound for the FCN amplitude, and the upper bound for α obtained from the out-of-phase component of the retrograde annual nutation, we estimate a lower bound for σ_ζ^2. Taking α to be $\leq 2\pi\times 3.3\times10^{-5}$ d^{-1} (99.5% confidence limit) [see *Gwinn et al.*(1986) for computation method], we find $\sigma_\zeta^2 \geq 5.8\times10^{-4}\Delta t$ mas^2, where Δt is in days. This lower bound for σ_ζ^2 indicates

TABLE 1. Estimates of Corrections to Amplitudes of Circular Nutations of IAU 1980 Nutation Series (*Wahr*, 1981).

Period in inertial space, days	Observed Amplitude, mas	Corrections*	
		In-Phase δa_r, mas	Out-of-Phase δa_i, mas
182.6 prograde	-548.63	0.44	-0.41
182.6 retrograde	-24.61	-0.09	-0.07
13.7 prograde	-94.43	-0.35	0.01
13.7 retrograde	-3.64	-0.02	0.04
365.3 prograde	25.73	0.07	0.15
365.3 retrograde	-33.12	-2.06	0.33
27.6 prograde	14.52	0.00	0.06
27.6 retrograde	-13.78	0.04	0.00
121.7 prograde	-21.58	-0.10	-0.03
121.7 retrograde	-0.96	-0.05	-0.04
9.1 prograde	-12.52	-0.09	0.00
9.1 retrograde	-0.45	0.01	-0.02
31.8 prograde	3.17	-0.03	-0.03
31.8 retrograde	-3.02	0.07	-0.01
433.2 prograde	0.04†	-0.03	-0.02
433.2 retrograde FCN	0.33†	0.32	-0.07

*The standard deviation of each correction is estimated to be 0.10 mas, except for those of the annual and 433-day terms whose standard deviations are estimated to be 0.12 mas. The standard deviations are obtained using the techniques described in *Herring et al.* (1986), with the root-sum-squares addition of a contribution of 0.07 mas to account for (i) the effects of the truncation of the IAU 1980 nutation series to the nearest 0.1 mas, (ii) the possible effects of atmospheric excitation of the nutation, and (iii) the effects of ocean and earth tide modeling errors in the analysis of the VLBI data. See also *Herring et al.* (1986) for definitions of the quantities listed.

†The amplitudes of these terms are the root-sum-squares of the amplitudes of the real and imaginary components.

that the complex amplitude of the FCN would have a variance $>(0.5 \text{ mas/year})^2$. (Although formally this estimate of the variance for the change in the complex amplitude of the FCN per year is a lower bound (due to our use of bounds in its calculation), our model probably predicts too much variation because of the assumed white-noise excitation which has a constant power-density, independent of frequency.) The VLBI estimates of the changes in both the FCN and the prograde signal are shown in Figure 2. The particular paths followed by each of these signals are not important. The important point is the absence of evidence that the single ("average") estimate of the amplitude of the FCN obtained from the VLBI data is greatly diminished by fluctuation in the complex amplitude of the FCN during the six-year interval spanned by the VLBI data. We also note that the average value of the amplitude of the FCN is consistent with our previous single estimate, and much smaller than the bound implied from the atmospheric-pressure data.

The results given in Table 1 and Figure 2 indicate that the amplitude of the FCN is no larger than 0.6 mas (99.5% confidence limit). The VLBI upper bound for the FCN amplitude thus suggests that the PSD of the excitation is no more than 0.06 $(\text{gm cm}^{-2})^2$ day (99.9% confidence limit), about five times smaller than that calculated by *Eubanks et al.* Since we have used an upper bound for the FCN amplitude and a lower bound for the damping, the actual PSD of the excitation

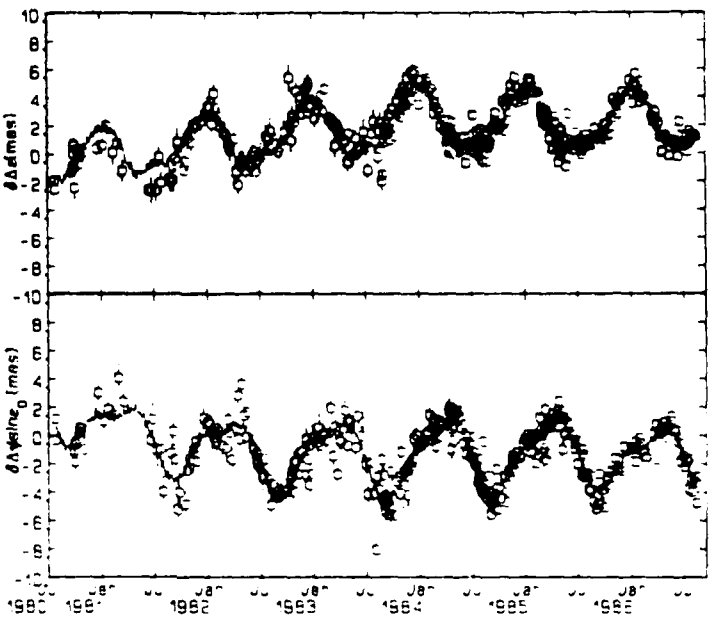

Figure 1. Estimates of $\delta\Delta\epsilon$ and $\delta\Delta\psi \sin\epsilon_0$ from the VLBI data analyzed in this paper. The solid line in each figure is computed from the corrections given in Table 1 and from long-period terms (periods $\geq$ 18.6 years) which are not given in the table because their values are highly correlated and the estimates are not considered reliable.

might be considerably less than the bound given.

4. CONCLUSION

Our analysis has placed an upper bound of 0.6 mas (99.5 % confidence limit) on the amplitude of the FCN. If the FCN is excited by surface loading with periods near one day, then this upper bound for the FCN amplitude combined with a lower bound for the damping time, allows an upper bound to be placed on the power-spectral density (PSD) of the surface loading. This upper bound for the surface loading is 0.06 $(\text{gm cm}^{-2})^2$ day (99.9 % confidence limit) which is about five times smaller than the estimate by *Eubanks et al.* of the PSD of the surface loading due to atmospheric pressure variations. These results suggest that this PSD is dominated by noise or that the excitation of the FCN by surface loading is not as efficient as currently believed (*Sasao and Wahr*, 1981).

5. ACKNOWLEDGMENTS

This work was supported by the Air Force Geophysics Laboratory, contract F-19628-86-K-0025; NASA grant NAG5-538; and NSF grant EAR-83-06380.

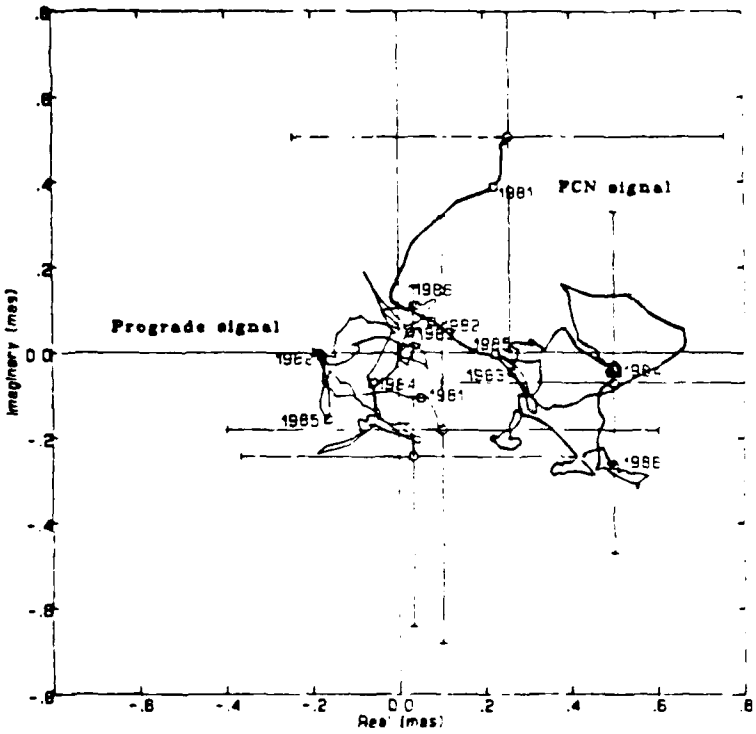

Figure 2. The estimates of the temporal changes in the complex amplitude of the FCN and the corresponding prograde terms, computed using the Kalman filter described in the text. The open squares show the values on January 1 for years between 1981 and 1986, as well as for the initial and final epochs for the data span. The error bars, shown only at the beginning and the end of the time interval spanned by the data, are one standard deviation, computed using the algorithm discussed in the caption of Table 1.

6. REFERENCES

Eubanks, T.M. *et al.*, in "Proc. of the international conference on earth rotation and the terrestrial reference frame", Ohio State University, 326–340, 1985.
Gwinn, C.R. *et al.*, *EOS*, **65**, 859, 1984.
Gwinn, C.R. *et al.*, *J. Geophys. Res.*, **91**, 4755–4765, 1986.
Herring, T.A. *et al.*, *EOS*, **64**, 674, 1983.
Herring, T.A. *et al.*, in "Proc. of the international conference on earth rotation and the terrestrial reference frame", Ohio State University, 307–325, 1985.
Herring, T.A. *et al.*, *J. Geophys. Res.*, **91**, 4745–4754, 1986.
Liebelt, P.B., "An introduction to optimal estimation", Addison-Wesley, 273, 1967.
Sasao, T. and J.M.Wahr, *Geophys. J. Roy. Astr. Soc.*, **64**, 729–746, 1981.
Wahr, J.M. and T.Sasao, *Geophys. J. Roy. Astr. Soc.*, **64**, 747–765, 1981.

DISCUSSION

Schuh: Why have you not entered the 22 nutation coefficients as solve for parameters in a global VLBI solution?

Reply by Herring: We haven't implemented the software yet to do that. We consider the nutation angle approach to be more flexible, as evidenced by our current paper.